

Supplementary information for:

**Accounting for species' thermodynamic activities changes mechanistic interpretations of electrochemical kinetic data**

Kindle Williams,<sup>a</sup> Aditya Limaye,<sup>a</sup> Trent Weiss,<sup>a</sup> Minju Chung,<sup>a</sup> Karthish Manthiram<sup>a,\*</sup>

<sup>a</sup> *Department of Chemical Engineering, Massachusetts Institute of Technology, Cambridge, MA 02139, United States*

\* *Corresponding author. Email: karthish@mit.edu*

## Table of Contents

List of Abbreviations .....	3
Materials .....	3
Methods: Electrolyte preparation.....	5
Methods: Electrochemical cells .....	6
Methods: RDE experiments.....	7
Methods: Preparation of RDE working electrodes .....	11
1. Gold disk <sup>3</sup> .....	11
2. Platinum disk <sup>4</sup> .....	12
Methods: Calibrating reference electrode.....	12
1. Calibrating vs. Master Ag/AgCl .....	12
2. Calibrating vs. ferrocene, decamethylferrocene .....	13
Methods: Headspace-GC-TCD.....	16
1. Sample preparation & equilibration.....	16
2. Sampling & detection .....	18
Methods: Linear regression.....	20
Raw data from main-text figures .....	21
Fig 2A: Water concentration-activity relationship for HER electrolyte.....	21
Fig 2C: Water dependence of HER at -1.875 V vs. Me <sub>10</sub> -Fc .....	21
Fig 4A: Water concentration-activity relationship for epoxidation electrolyte .....	21
Fig 4B: Water concentration-activity relationship for lactonization electrolyte .....	22
Fig 4C: Water dependence of cyclooctene epoxidation at 1.45 V vs. Fc .....	22

## Supplementary Information

Fig 4D: Water dependence of cyclohexanone lactonization.....	22
Discussion: Measured activity curves overlaid on one another.....	23
Discussion: Faradaic efficiency of HER.....	24
Reference: Volmer, Tafel, and Heyrovsky steps .....	25
Discussion: TST reaction rate expression formulation.....	25
A note on “hot” reactants and other thermodynamic exceptions.....	27
Discussion: HER on Pt cathode .....	27
Reference: Tafel slopes.....	28
Discussion: Confirming lack of transport limitations in RDE measurements.....	29
Discussion: ET potential scales versus CPET potential scales (Measurement of RHE in blended electrolyte) .....	31
Water dependence at a constant V vs. RHE .....	36
Discussion: pH effect on HER.....	39
Discussion: Experimental troubleshooting & minimizing background current .....	39
Discussion: Local Tafel slopes & sensitivity of Tafel slope to fit range .....	41
Discussion: Water dependences of HER in blended electrolyte at different potentials .....	42
Discussion: Sources of errors (accounted and unaccounted) in HER water dependence data .....	44
Discussion: On curvature in order-dependence data .....	45
Discussion: Water movement across the glass frit .....	46
Discussion: Effect of water content on organic substrate activity for OAT reactions.....	47
SI References .....	47

**List of Abbreviations**

- ACN: acetonitrile
- CA: chronoamperometry
- CV: cyclic voltammetry
- EtOH: ethanol
- Fc: ferrocene
- FE: Faradaic efficiency
- GC: gas chromatograph
- HER: hydrogen evolution reaction
- HS: headspace
- IPA: isopropyl alcohol
- LSV: linear sweep voltammetry
- Me<sub>10</sub>-Fc: decamethyl ferrocene
- MIR: manual IR-drop (Ohmic drop) correction
- OCV: open circuit voltage
- ORR: oxygen reduction reaction
- PEIS: potentiometric electrochemical impedance spectroscopy
- RDE: rotating disk electrode
- RHE: reversible hydrogen electrode
- SHE: standard hydrogen electrode
- SWV: square wave voltammetry
- TBABF<sub>4</sub>: tetrabutylammonium tetrafluoroborate
- TCD: thermal conductivity detector

**Materials**

Acetonitrile was purchased with a variety of specifications from a number of vendors and used interchangeably (Alfa Aesar anhydrous 42311, Alfa Aesar 43166, Sigma-Aldrich anhydrous 99.8% 271004), with drying by 3Å molecular sieves (4-8 mesh, Acros Organics) prior to use. Ultra-pure water was produced on-site by a Milli-Q® Integral Water Purification System purchased through EMD Millipore. Tetrabutylammonium tetrafluoroborate (TBABF<sub>4</sub>, TCI Chemicals T0914), tetrabutylammonium hydroxide (TBAOH, 40 wt% (1.5 M) in water, Acros Organics 176612500), ferrocene (Fc, 99%, powder, Alfa Aesar 87202), decamethyl ferrocene (Me<sub>10</sub>-Fc, 99%, crystalline, Beantown Chemical 142350), cis-cyclooctene (cyclooctene, 95%, stabilized, Alfa Aesar A13477), cyclohexanone (≥99.0%, Sigma-Aldrich 398241), sulfuric acid (H<sub>2</sub>SO<sub>4</sub>, 93-98%, TraceMetal grade, Fisher Scientific A510-P212), nitric acid (HNO<sub>3</sub>, 67-70%, TraceMetal grade, Fisher Scientific A509-P212), potassium hydroxide (KOH, ≥85%, pellets, Sigma-Aldrich 30603), ethanol (EtOH, 200 proof anhydrous, Koptec V1001), acetone (VWR, BDH1101-4LP and Fisher Chemical A18(P)-4), argon gas (Ar, 99.999%, Airgas AR UHP300, delivered via gas manifold), and hydrogen gas (H<sub>2</sub>, 99.999%, Airgas HY UHP300, delivered via gas manifold) were purchased and used as-received. Electrolyte solutions were stored in colorless

## Supplementary Information

polypropylene containers (VWR) and/or Corning® centrifuge tubes (VWR 430828 & 430790, 50 mL and 15 mL, respectively).

The gold disk electrode (Au, Pine Research #AFED050P040AU) and platinum disk electrode (Pt, Pine Research #AFED050P040PT) were polished using a polishing kit from CH Instruments (CHI120) along with a pre-made alumina slurry (0.3  $\mu\text{m}$ , Electron Microscopy Sciences #50368-20), while platinum wire electrodes (Pt, 99.995% trace metals basis, 0.25 mm diameter, Beantown Chemical 220450) and platinum foils (Pt, 99.99% trace metals basis, 0.025 mm thick, Beantown Chemical 213815) were rinsed and used as-received. The leak-free Ag/AgCl reference electrode (Innovative Instruments 3.4 M KCl, model LF-2) was stored in Milli-Q® water after opening. The master Ag/AgCl electrode (saturated KCl, CH Instruments CHI111) was stored in saturated KCl solution.

The H-cell used in most experiments was custom-made by JamesGlass, with 24/40 ground-glass joints on top. The compression O-ring for sealing around the reference electrode (Markez, size 201, Marco Rubber Z1028) was shaved down to a non-standard size in order to allow for a full seal. The gas-purged bearing used for sealing the working compartment was purchased from Pine Research (#AC01TPA6M). The sandwich cell used for FE closure and RHE measurement experiments was a two-compartment PEEK cell of the same type and dimensions as has been previously described in our work.<sup>1</sup> Plugs and connections that served as the sandwich cell parts were made of polypropylene, while ferrules were made of ETFE (Tefzel™); these parts were purchased from IDEX Health & Science. O-rings to seal the compartments upon assembly were made of FEP-Encapsulated Silicone (9319K15 & 9319K142) and were purchased from McMaster-Carr. Tubing for conveying gas flow was a mixture of 1/8" and 1/16" FEP tubing (Cole-Parmer, EW-06406). Aluminum foil used as a current collector for the sandwich cell was commercially available Reynolds Wrap.

A 16-channel BioLogic VMP3 potentiostat with EIS capabilities was used for all electrochemical experiments. Rotating Disk Electrolysis was carried out using a Pine Research WaveVortex 10 Rotator. Headspace-gas chromatography was conducted using an Agilent 7890B gas chromatograph with 7697A headspace sampler unit (12-vial); samples were prepared in 20 mL clear vials with crimp caps. The Agilent GC was outfitted with a DB-624UI column (30 m, 0.32 mm, 1.80  $\mu\text{m}$ , Agilent US0613613H) and a 7890 Thermal Conductivity Detector (TCD, w/EPC, Agilent G00VTJ). In-line gas detection of hydrogen was conducted using an SRI gas chromatograph (SRI Instruments, Inc., Model 8610C, MG 5 configuration with HayesepD and MS5A columns). Gas flows were regulated with Alicat flow controllers of varying specifications (e.g. MS-100SCCM-D/5M, GAS: Air; accurate to 1 decimal place in sccm). Electrolyte water content was tested using a Karl Fischer titrator (Mettler Toledo C10S Coulometric KF titrator). For sonication, VEVOR PS-10A (2 L; 60 W, 40 kHz) Ultrasonic Cleaners were used interchangeably with a VWR Symphony™ (97043-992; 90 W, 35 kHz) Ultrasonic Cleaner. For drying sieves, a muffle furnace (Thermo Scientific FB1315M) was used. A balance (VWR 164AC) was used to weigh all solids, and a mix of VWR and Fisherbrand pipettes (between 2-20  $\mu\text{L}$  and 1-5 mL) was used to measure out liquids.

**Methods: Electrolyte preparation**

Electrolytes for electrochemical experiments as well as headspace experiments were prepared from a combination of the following stock solutions:

1. Acetonitrile, dried over 5A Molecular Sieves
  - Anhydrous acetonitrile direct from the supplier was removed and pipetted into a 250 mL polypropylene stock bottle, where it was stored over 5A molecular sieves at a ratio of about 10% molecular sieves by volume.
  - Molecular sieves were regenerated periodically to maintain low moisture content by:
    - i. Pouring off any residual acetonitrile
    - ii. Rinsing sieves in acetone to remove organic contaminants
    - iii. Rapidly evaporating residual acetone on the sieves by leaving sieves in a negative-pressure location such as in a hood or under a snorkel, until sieves returned to original light tan color
    - iv. Transferring sieves to a ceramic crucible
    - v. Heating sieves in a general-use muffle furnace with the following temperature program:
      1. Ramp: Room Temperature  $\rightarrow$  350 °C at rate of 15 °C/min (20 min ramp)
      2. Hold at 350 °C for 4 hours
      3. Shut off program at 4 hours and allow to cool naturally
    - vi. Retrieving the sieves after ~30 minutes and returning them to a dry, solvent-free 250 mL polypropylene stock bottle
    - vii. Adding fresh acetonitrile
    - viii. Stirring/shaking bottle gently
    - ix. Allowing solvent to sit like this overnight prior to using
  - Water content of stock acetonitrile was tested periodically by Karl Fischer titration. Sieves consistently kept water content undetectable (<100 ppm water given a ~0.5 mL sample of acetonitrile).
2. Milli-Q water
  - Obtained directly from the lab Milli-Q unit; stored temporarily in a 50 mL polypropylene falcon tube.
3. 1.0 M TBABF<sub>4</sub> in acetonitrile
  - Because of the bulkiness of the tetrabutylammonium cation in solution, 1.0 M TBABF<sub>4</sub> was prepared by adding enough TBABF<sub>4</sub> powder to produce the desired molarity, then dissolving it in enough acetonitrile to lead to the desired solution volume. For 100 mL of 1.0 M TBABF<sub>4</sub>, the formulation was found to be:
    - i. 32.93 grams TBABF<sub>4</sub> (= 0.1 mol)
    - ii. 67.5 mL acetonitrile (= 53.055 g = 1.292 mol at room temperature)
  - It may be noted that this implies TBABF<sub>4</sub> in acetonitrile takes up space in such a manner that it adds ~1 mL/gram TBABF<sub>4</sub>.
  - The stock solution is 7.18 mol% TBABF<sub>4</sub> and 92.82 mol% acetonitrile.

## Supplementary Information

4. 100 mM ferrocene in acetonitrile
  - 372.1 mg ferrocene in 20 mL acetonitrile
5. 5 mM decamethyl ferrocene in acetonitrile
  - Added 21.2 mg decamethyl ferrocene to 13 mL of sieve-dried acetonitrile. Vortexed/sonicated to dissolve. This is right at / slightly above the solubility limit of decamethyl ferrocene in acetonitrile, so some decamethyl ferrocene powder may persist in solution.

Note that, while volume changes were accounted for in solution (3), volume changes due to mixing were ignored for the combination of any of these stock solutions with one another. Visually, volumes were observed to be consistent, suggesting this approximation contributed very little error (certainly <5%) to reported molarities. See below for solution formulations.

### Methods: Electrochemical cells

The electrochemical cell used in RDE experiments was a custom 2-compartment glass H-cell by JamesGlass. The two compartments were separated by a glass frit, and each compartment was equipped at the top with a female 24/25 ground glass joint. Total electrolyte volume used in experiments, in order to fully cover the glass frit, was 30 mL. A horizontal glass threaded fitting on the working compartment allowed for the use of a reference electrode. A leak-free Ag/AgCl in 3.5 M KCl reference was inserted into this fitting and sealed using a compression O-ring (Markez, size 201, shaved down to non-standard size allowing full seal on the reference electrode). The O-ring fitting was finger-tightened as much as possible to maintain a seal against the electrolyte. The cell was cleaned prior to all experiments by a dip in 20% nitric acid, and between experiments was cleaned with Milli-Q water & acetone rinses.



Figure S1. Photo of H-cell used in electrochemical experiments. Custom cell by JamesGlass.

**Methods: RDE experiments**

Prior to every RDE experiment, the reference electrode was calibrated (see *Methods: Calibrating Reference Electrode – 1. Calibrating vs. Master Ag/AgCl*) and the working electrode was cleaned and prepared according to literature-based procedures (see *Methods: Preparation of RDE Working Electrodes*). In addition, the custom 2-compartment glass H-cell with reference port – cleaned from any prior experiments – was removed from an 80 °C oven where it had been drying. After the glass electrochemical cell had cooled close to room temperature and the calibrated leak-free Ag/AgCl had been inserted, the relevant electrolyte was added to each compartment to entirely cover the glass frit. See table below for formulation of basic electrolytes.

Table S1. Electrolyte formulations for RDE experiments in H-cell.

<b>Solution</b>	<b>0.5 M H<sub>2</sub>O</b>	<b>1 M H<sub>2</sub>O</b>	<b>2.5 M H<sub>2</sub>O</b>	<b>5 M H<sub>2</sub>O</b>	<b>6.6 M H<sub>2</sub>O</b>
Volume Water	--	270 $\mu$ L	1.08 mL	2.43 mL	3.28 mL
Volume TBAOH	451 $\mu$ L	451 $\mu$ L	451 $\mu$ L	451 $\mu$ L	451 $\mu$ L
Volume Fresh ACN	6.22 mL	5.95 mL	5.14 mL	3.79 mL	2.93 mL
Volume 1.0 M TBA/ACN	23.32 mL	23.32 mL	23.32 mL	23.32 mL	23.32 mL

After adding the electrolyte to the cell, 1/16" FEP tubing was used to bubble Argon gas into the working electrolyte at a rate of 20 sccm for at least 10 minutes to purge the electrolyte of dissolved oxygen gas. A brief purge of the counter electrolyte was also sometimes conducted. Immediately after the electrolyte purge, the rotator shaft with working electrode was lowered into the working compartment of the H-cell, and a Pine Gas-Purged Bearing was used to seal the working compartment. The Ar line was reconnected to direct 20 sccm Ar through this bearing, maintaining an inert Ar atmosphere in the working compartment headspace. The three-electrode setup was completed by inserting a Pt wire into the counter compartment and attaching it to the potentiostat cables. At this point the enclosure was lowered, the rotator set to spin at 1600 rpm, and the local exhaust ventilation put in place. The setup was then ready for electrolysis.

## Supplementary Information

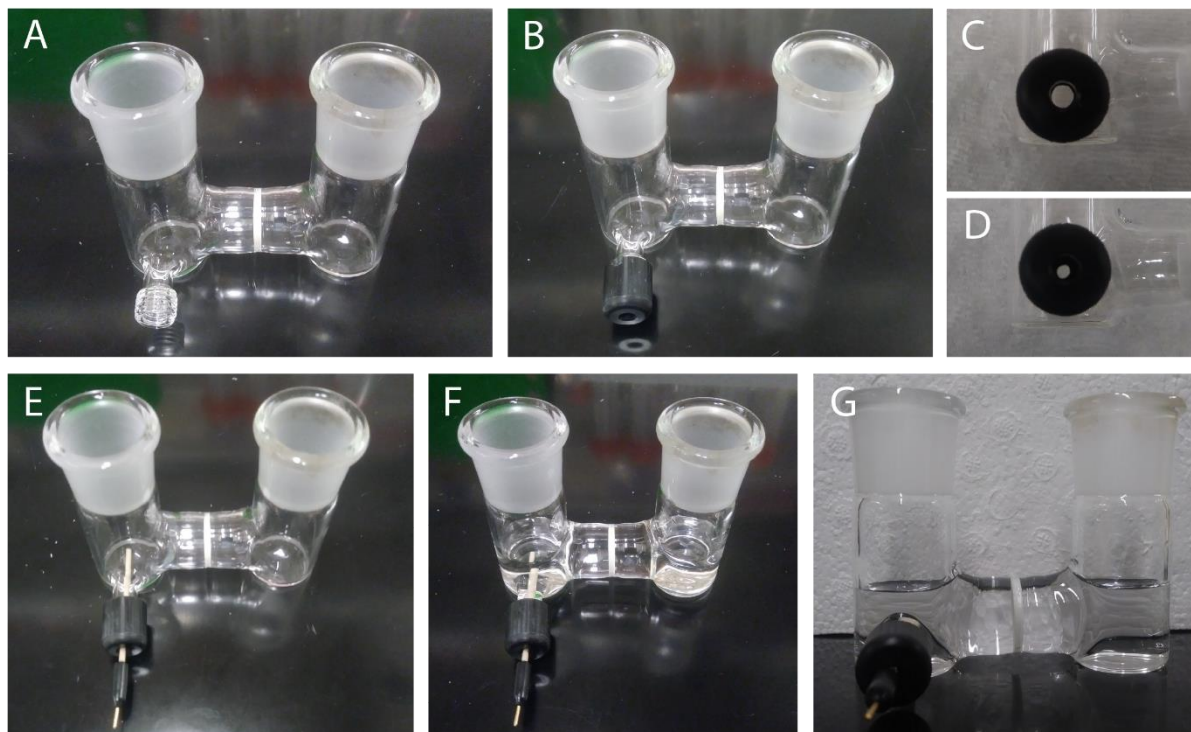


Figure S2. Assembly and loading of H-Cell. A) H-Cell taken directly from drying oven. B) H-Cell with addition of compression O-ring and compression fitting on reference port. C) O-ring/reference port prior to tightening fitting. D) O-ring/reference port after slightly tightening fitting – note O-ring compression. E) Full cell with reference inserted into port. F) Full cell after loading with 30 mL electrolyte. G) Front-on image of full cell after loading with 30 mL electrolyte.

## Supplementary Information



Figure S3. Insertion of prepared disk into RDE assembly. A) Polished Au disk. B) Disk in PTFE casing at the rotator shaft tip. C) Assembly in (B) inserted into the outer PEEK shroud. D) Pushing down the assembly in (C) to properly seat the Au disk into the PEEK shroud. E) Image of the result of proper seating. F) Side-profile image of the same. G) Dropping a plastic spacer into the back of the assembly. H) Screwing in the disk contact stud to enable electrical connection to the working electrode. I) The electrode tip assembly, ready to insert onto the rotator shaft. J) The electrode tip assembly from a different angle. K) Preparing to insert the electrode tip into the rotator shaft. L) Seating the electrode assembly into the rotator & screwing in. M) Final assembly, including gas-purged bearing attached to rotator shaft. N) Wider view of final assembly, now ready to use.

## Supplementary Information

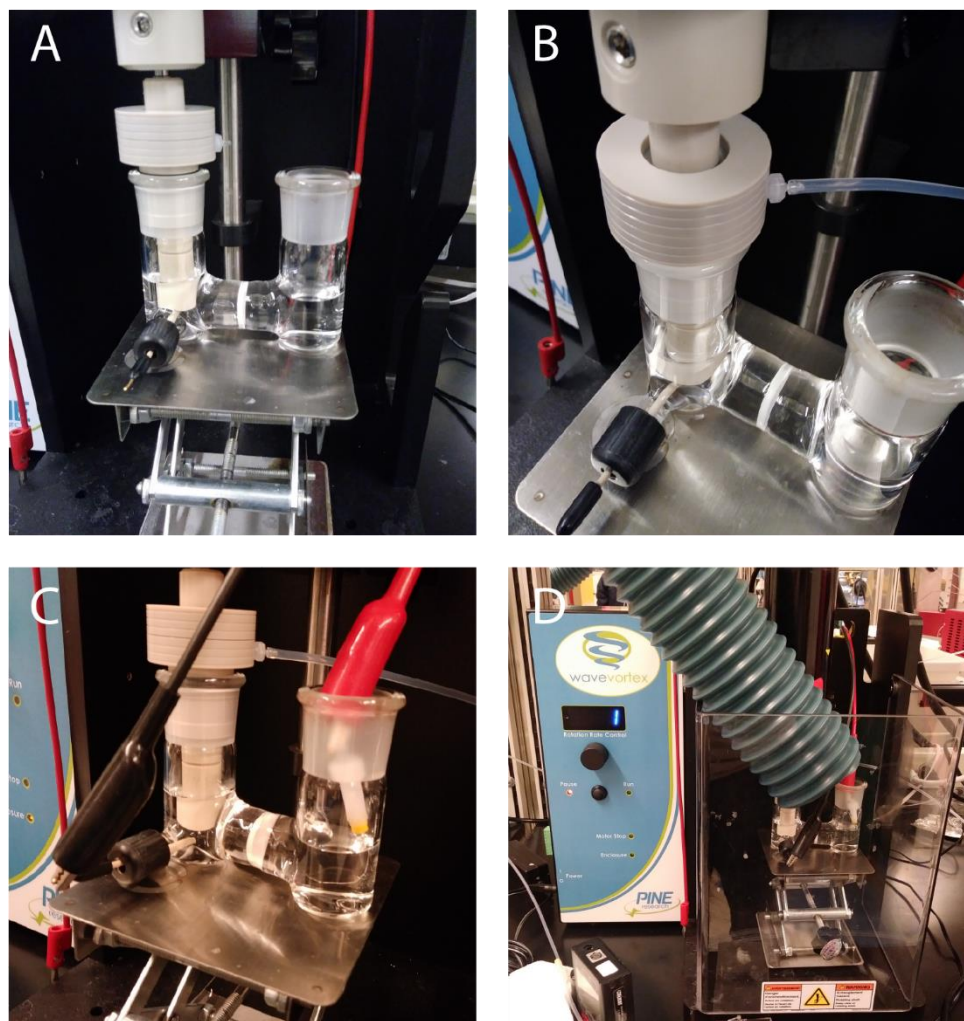


Figure S4. Combining the prepared H-cell with the prepared electrode to finalize setup. A) RDE inserted into working compartment of filled H-cell. B) Argon gas line connected to gas-purged bearing. C) Counter electrode inserted into counter compartment, and electrodes hooked up to potentiostat. D) Final setup complete with local exhaust ventilation.

For a typical HER experiment, the following EC-Lab sequence was run:

1. PEIS: 200 kHz – 1 Hz
2. Pause
3. MIR: Correct for  $[R_{\text{measured}}]$  at 85%
  - Resistance was measured as the x-intercept of EIS data, to the nearest Ohm. Usually ~15 Ohm total.
4. LSV: -0.5 V to -2.0 V vs. Ag/AgCl
  - 10 mV/sec scan rate

## Supplementary Information

- Initial LSV gave a sense for the required sweep windows and hold potentials in subsequent steps.
5. CA: hold at  $[V_{\text{ORR}}]$  for 30 minutes
    - To remove any residual oxygen from the system, the working electrode was held at a potential at which only the oxygen reduction reaction (ORR) was taking place. A typical value was -1.5 V vs. Ag/AgCl. Over the course of the half-hour hold, the remaining oxygen in the cell was depleted through reaction. Water produced by ORR during the experiment was considered to be negligible in comparison to the amount of water explicitly added to the system, due to the low solubility of oxygen gas in acetonitrile.<sup>2</sup>
  6. LSV: -0.5 V to -2.0 V vs. Ag/AgCl
    - 2 mV/sec scan rate – nearly steady-state measurements at every potential, with very little contribution due to capacitance
  7. CA: hold at -1.9 V vs. Ag/AgCl for 30 minutes
    - To assess stability of current at any given potential
  8. OCV for 1 min
  9. PEIS: 200 kHz – 1 Hz
    - Confirm no change in resistance
  10. LSV: -0.5 V to -2.0 V vs. Ag/AgCl
    - 10 mV/sec scan rate
    - Duplicate fast LSV with no oxygen
  11. CA: hold at  $[V_{\text{ORR}}]$  for 5-10 minutes
    - Confirm no increase in ORR background
  12. LSV: -0.5 V to -2.0 V vs. Ag/AgCl
    - 2 mV/sec scan rate
    - Duplicate slow LSV
  13. CA: hold at -1.9 V vs. Ag/AgCl for 30 minutes
    - To assess recovery of current at any given potential

Data from these experiments was processed in order to:

- Manually correct for the remaining 15% IR drop that was uncompensated during the experiment
- Plot as  $\log(i)$  vs.  $V$ , a.k.a. as a Tafel plot
- Make a cut at constant  $V$  vs. Me<sub>10</sub>-Fc across all values of water content, using the calibration of the Ag/AgCl reference versus Me<sub>10</sub>-Fc.

### Methods: Preparation of RDE working electrodes

#### 1. Gold disk<sup>3</sup>

The Au disk (Pine Research #AFED050P040AU) was prepared by first removing any visible residue from prior experiments by rinsing with acetone and water. The Au was then

## Supplementary Information

placed in a PTFE disk polishing holder and hand-polished, in some cases with 0.3  $\mu\text{m}$  alumina on a vinyl pad reserved for use with Au (30 sec – 2 min), and in all cases finishing with a fine 0.05  $\mu\text{m}$  alumina MicroPolish on a microfiber pad reserved for use with Au (2 min). Following the 0.05  $\mu\text{m}$  polish, the Au disk was removed from the holder and placed in a 15 mL Falcon tube, to which was added ~2 mL of 50:50 Milli-Q water:acetone by volume. The disk was sonicated using a VWR Symphony™ (97043-992; 90 W, 35 kHz) Ultrasonic Cleaner in the water/acetone mixture for at least 2 minutes, then the water/acetone mixture was decanted, more 50:50 water:acetone was added, and one more sonication cycle of 2+ minutes was initiated. At this point the Au disk was retrieved and inserted into the RDE assembly with Kimwipes and relatively clean gloves.

Finally, the Au disk was electro-polished by inserting the RDE into a beaker cell (10 mL beaker volume) containing ~1 mL of 0.1 M  $\text{H}_2\text{SO}_4$  and running a 200x cycled oxidative CV between 0 and +1.800 V vs. the counter electrode at a scan rate of 1 V/sec. In this case the counter electrode was a Pt wire. The chosen voltage window was selected to correspond to roughly 0 to +1.700 V vs. SHE. The rotator was spun at a rotation rate of 600 rpm during these oxidative cycles. Following the completion of this 200x oxidative cycling in 0.1 M  $\text{H}_2\text{SO}_4$ , the working electrode was rinsed twice with Milli-Q water and any residual water remaining on the electrode was gently wicked away using a Kimwipe. At this point the disk was ready for use in an electrochemical experiment.

### 2. *Platinum disk*<sup>4</sup>

Pt disks (Pine Research #AFED050P040PT) were handled in a similar manner to Au disks, with the differences being:

- During sonication, a 50:50 v/v mixture of Milli-Q and ethanol was used, rather than 50:50 water:acetone.
- During electro-polishing, the  $\text{H}_2\text{SO}_4$  electrolyte was 0.5 M  $\text{H}_2\text{SO}_4$  rather than 0.1 M.
- Also during electro-polishing, the oxidation was split out into two steps, with replacement of the 0.5 M  $\text{H}_2\text{SO}_4$  electrolyte in-between:
  1. 2-minute hold at +2.1 V vs. counter (est. +2.0 V vs. SHE)
  2. 10x CV from 0 to 1.40 V vs. counter (est. +1.35 V vs. SHE) at 50 mV/sec

## Methods: Calibrating reference electrode

### 1. *Calibrating vs. Master Ag/AgCl*

Prior to most experiments, reference stability and drift were assessed by calibration versus a “Master” Ag/AgCl reference in saturated KCl. This Master was not used in electrochemical experiments, and was stored in saturated KCl in Milli-Q water. To calibrate, the Master reference and the leak-free Ag/AgCl reference being calibrated were

## Supplementary Information

placed in the same vial filled with saturated KCl. The reference being calibrated was hooked up as the Working Electrode, and the Master was hooked up as the Counter/Reference Electrode. OCV was then measured until drift over time had decreased substantially below 1 mV – often for around an hour. The final “plateau” OCV was recorded and used to gauge reference drift between experiments, correcting for small changes from run to run. For example: if a leak-free reference had been calibrated as +0.100 V vs. Master Ag/AgCl, and simultaneously +0.020 V vs. Me<sub>10</sub>-Fc in the relevant solvent being tested, and then on a subsequent experiment the reference was measured to be +0.105 V vs. Master, then that reference was interpreted as representing +0.025 V vs. Me<sub>10</sub>-Fc. Historical calibration data – with two or more ferrocene calibrations separated by multiple measurements of drift vs. a Master – corroborate the accuracy of this approach to drift correction.

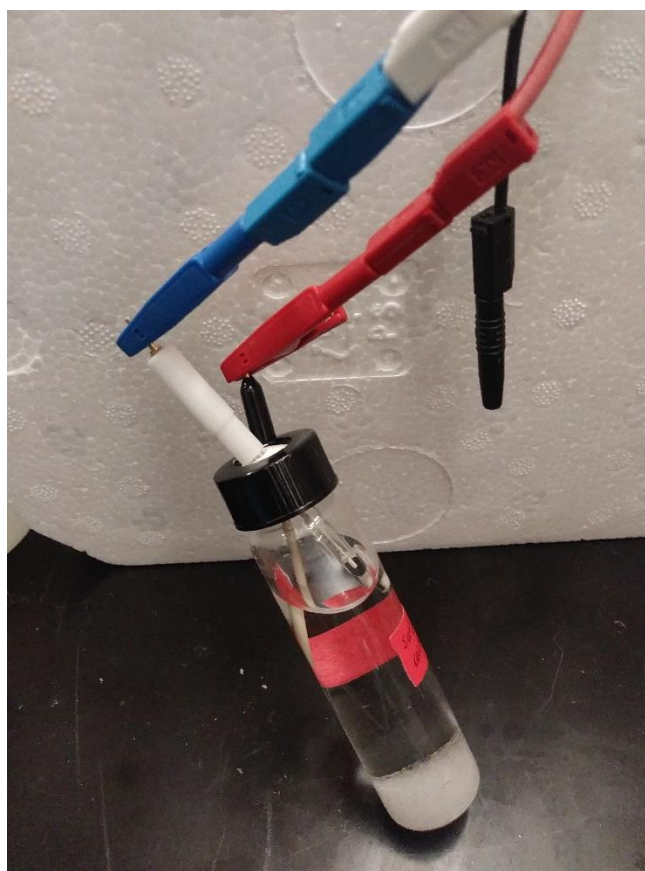


Figure S5. Calibrating leak-free Ag/AgCl reference electrodes versus a Master Ag/AgCl reference in saturated KCl solution.

### 2. *Calibrating vs. ferrocene, decamethylferrocene*

## Supplementary Information

Reference electrodes were calibrated simultaneously versus both Fc and Me<sub>10</sub>-Fc by preparing solutions that were roughly 2.5 mM in both redox standard species. Other than Fc/Me<sub>10</sub>-Fc content, solutions were prepared to reflect the conditions (water content) of each HER water dependence test. The following table reflects the compositions of the 4-mL electrolytes used for calibration:

Table S2. Formulations of solutions used in Fc/Me<sub>10</sub>-Fc calibrations.

<b>Solution</b>	<b>0 M H<sub>2</sub>O</b>	<b>0.5 M H<sub>2</sub>O</b>	<b>1 M H<sub>2</sub>O</b>	<b>2.5 M H<sub>2</sub>O</b>	<b>5 M H<sub>2</sub>O</b>	<b>6.6 M H<sub>2</sub>O</b>
<b>TBABF<sub>4</sub> powder</b>	1.0527 g (1.0537 g)	1.0214 g (1.0248 g)	1.0242 g (1.0248 g)	1.0252 g (1.0248 g)	1.0258 g (1.0248 g)	1.0253 g (1.0248 g)
<b>100 mM Fc Stock</b>	100 $\mu$ L	100 $\mu$ L	100 $\mu$ L	100 $\mu$ L	100 $\mu$ L	100 $\mu$ L
<b>5 mM Me<sub>10</sub>-Fc Stock</b>	2 mL	2 mL	2 mL	2 mL	2 mL	2 mL
<b>Milli-Q Water</b>	--	--	36 $\mu$ L	144 $\mu$ L	324 $\mu$ L	438 $\mu$ L
<b>Fresh ACN</b>	846 $\mu$ L	815 $\mu$ L	779 $\mu$ L	671 $\mu$ L	491 $\mu$ L	377 $\mu$ L
<b>40% (1.5 M) TBAOH</b>	--	60.1 $\mu$ L	60.1 $\mu$ L	60.1 $\mu$ L	60.1 $\mu$ L	60.1 $\mu$ L

Solutions were tested in a randomized order (achieved via an online random number generator). For each solution, ~2 mL was added to a 10 mL beaker containing a Pt wire that served as the counter electrode. The working electrode was a Pt RDE disk on the WaveVortex 10 rotator. This electrode had been rinsed with water and acetone prior to the experiment, and dried of all solvent prior to insertion into the electrolyte being tested. During the experiment, the rotator was spun at a rotation rate of 900 rpm.

To ascertain the potential of the reference electrode versus the redox of Fc and Me<sub>10</sub>-Fc species in solution, square wave voltammetry (SWV) was used. The SWV started with an initial oxidative pre-hold on the working electrode at 0 V vs. Ag/AgCl for 20 seconds, followed by a scan down to roughly -0.300 V vs. Ag/AgCl, and then a return to the initial potential of 0 V vs. Ag/AgCl. This was repeated twice, once with an initial hold at the reductive potential (-0.300 V vs. Ag/AgCl), and again with an initial hold at the oxidative potential (0 V vs. Ag/AgCl). Because the cleanest data was obtained for the first scan, only results from the first SWV for each composition is reported here. In these tests, the pulse height was 50 mV; pulse width was 100 ms; step height was (+/-)1 mV; and *I* was averaged over the last 20% of the step. The potentiostat Erange was -1 – 1 V, Irange 10 mA, and bandwidth medium. Note the SWV voltage window was shifted as necessary to contain peaks for both the Fc and Me<sub>10</sub>-Fc redox events in any given electrolyte. In addition, 85% software IR correction was implemented during the experiment.

## Supplementary Information

Potentials were determined by identifying the peak potential on a plot of  $I_{\text{delta}}$  vs.  $E_{\text{step}}$ , and averaging the peaks in the oxidative and reductive directions.

It should be noted that for lower water content (0 - 1 M water), stable measurements past the initial SWV were difficult, so for each experiment (including those at higher water content, for consistency) only the first SWV was used for peak-potential-averaging.

Following each electrolyte measurement, the electrolyte was removed and discarded, and the working electrode and rotator were rinsed with acetone and Milli-Q water, while the beaker cell and counter electrode were rinsed with dry acetonitrile. Trace acetonitrile was removed from the beaker cell, and then the next electrolyte in the sequence was inserted and tested.

The following figures show results of this calibration.

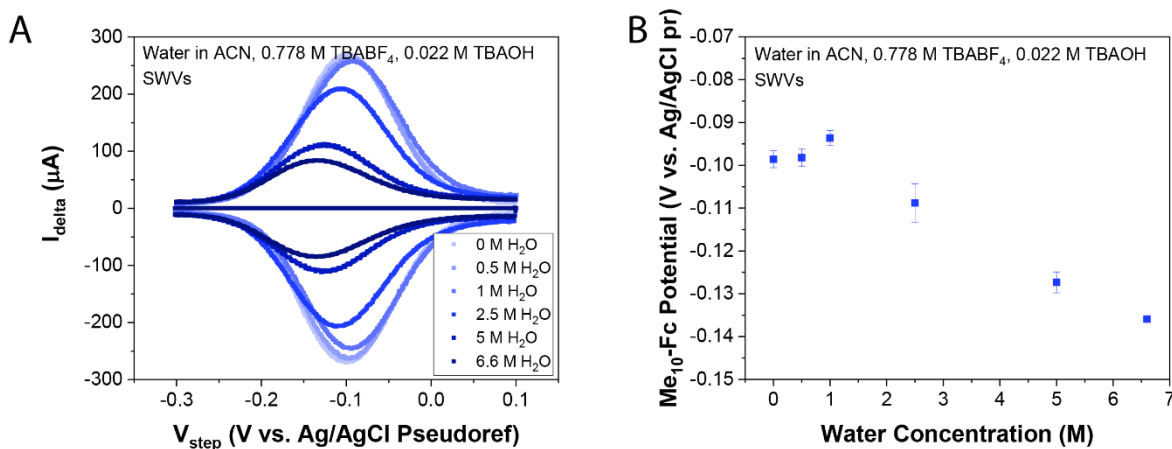


Figure S6. Me<sub>10</sub>-Fc calibration in alkaline ACN electrolyte. Note that Fc was more difficult to calibrate in base due to overlapping OER / other pH-sensitive oxidative chemistries. A) Raw data from Me<sub>10</sub>-Fc calibrations across water content. Darker lines correspond to higher water content. Note the decreasing solubility of Me<sub>10</sub>-Fc is reflected by the decrease in SWV peak height with increasing water content. B) Me<sub>10</sub>-Fc calibration data.

In addition, calibrations were also conducted in neutral electrolytes consisting of ACN, water, and 0.8 M TBABF<sub>4</sub> in the absence of TBAOH. Slightly different SWV settings were used for these scans (voltage window +0.700 V vs. Ref – -0.300 V vs. Ref, pulse height 25 mV, pulse width 50 ms, step height (+/-)2 mV, E range -2 – 2 V). These neutral calibrations yielded similar results to those in base. Note the shifting of the leak-free Ag/AgCl pseudoreference electrode over time led to a shift in the y-axis that is not reflective of thermodynamic shifts between the alkaline and neutral conditions, but rather of changes in the pseudoreference itself in the weeks/months between the neutral and alkaline tests.

## Supplementary Information

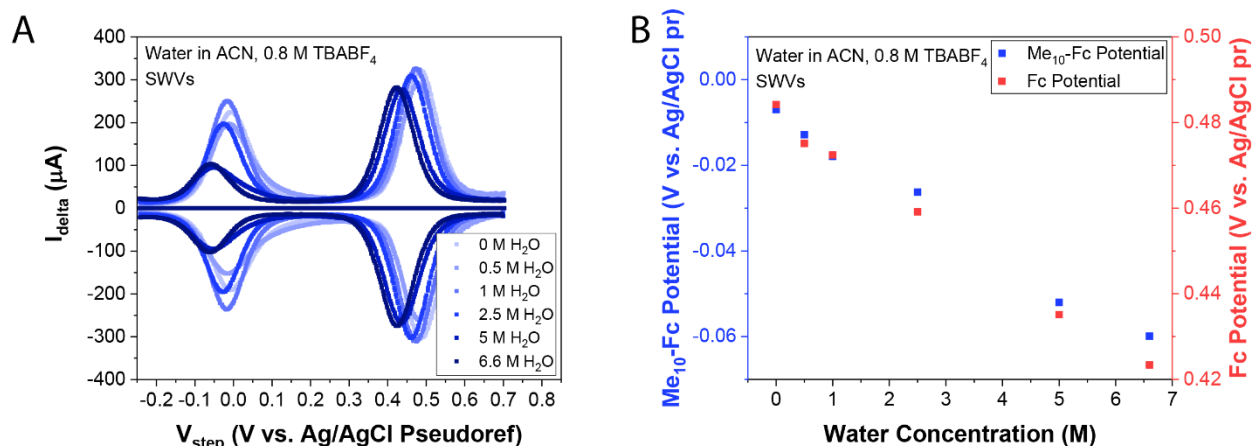


Figure S7. Simultaneous Me<sub>10</sub>-Fc and Fc calibration in neutral ACN electrolyte. A) Raw data from Fc/Me<sub>10</sub>-Fc calibrations across water content. Darker lines correspond to higher water content. B) Fc/Me<sub>10</sub>-Fc calibration data. Note that there is a similar shift in both Fc and Me<sub>10</sub>-Fc vs. the Ag/AgCl pseudoreference.

### Methods: Headspace-GC-TCD

Species thermodynamic activities were measured by sampling from the headspace of vials containing electrolyte with a specified water content. This was achieved using an Agilent 7890B GC with 7890A Thermal Conductivity Detector and attached 12-vial 7697A Headspace Sampler. These experiments can be broken down into two components: 1) sample preparation and equilibration, and 2) sampling and detection.

#### 1. Sample preparation & equilibration

Electrolyte samples were prepared in 20 mL headspace vials, with liquid sample volumes of 4 mL. Sample formulation was according to the following table:

Table S3. Formulations of 4-mL basic electrolytes for headspace sampling.

Solution	0 M H <sub>2</sub> O	0.5 M H <sub>2</sub> O	1 M H <sub>2</sub> O	2.5 M H <sub>2</sub> O	5 M H <sub>2</sub> O	6.6 M H <sub>2</sub> O	Sat'd H <sub>2</sub> O
Volume Water	--	--	36 µL	144 µL	324 µL	438 µL	600 µL
Volume TBAOH	--	60.1 µL	60.1 µL	60.1 µL	60.1 µL	60.1 µL	60.1 µL
Volume Fresh ACN	800 µL	829 µL	793 µL	685 µL	505 µL	391 µL	229 µL
Volume 1.0 M TBA/ACN	3.2 mL	3.11 mL	3.11 mL	3.11 mL	3.11 mL	3.11 mL	3.11 mL

## Supplementary Information

It should be noted that these samples included two conditions – 0 M and saturated (~8.3 M) water – which did not represent electrolysis conditions, but rather served as the endpoints on the concentration-activity relationship, including a “blank” measurement.

For each sample, the vial for the sample was first stored overnight in an 80 °C oven to fully dry the glass and remove any adventitious water. The vial was then rapidly cooled to room temperature by air-cooling in a snorkel vent, and the sample components were added to the vial via pipette. The vial was then sealed with a Silver Aluminum 20 mm headspace crimp cap with PTFE/silicone stopper. Sealing was done using an Agilent manual crimper for 20 mm caps. The seal was such that the cap did not easily rotate on the vial when twisted, but the cap was also not visibly deformed around the stopper due to over-tightening. 3 sets of samples were prepared in this manner. Within each set, samples were prepared in a randomized order, specified by an online random number generator.

In addition to all electrolyte samples, a pure-water reference sample was prepared for each sample – with the intention being that a reference could be gathered before and after each electrolyte sample, providing a standard for water activity = 1 at every time point, i.e. at every value of room temperature.

After sealing, each sample was equilibrated at room temperature (~23 °C) for at least 12 hours. This threshold is supported by equilibration tests on electrolytes containing only water (see below). Water peak area reached its equilibrium value by roughly  $t = 8$  hours.

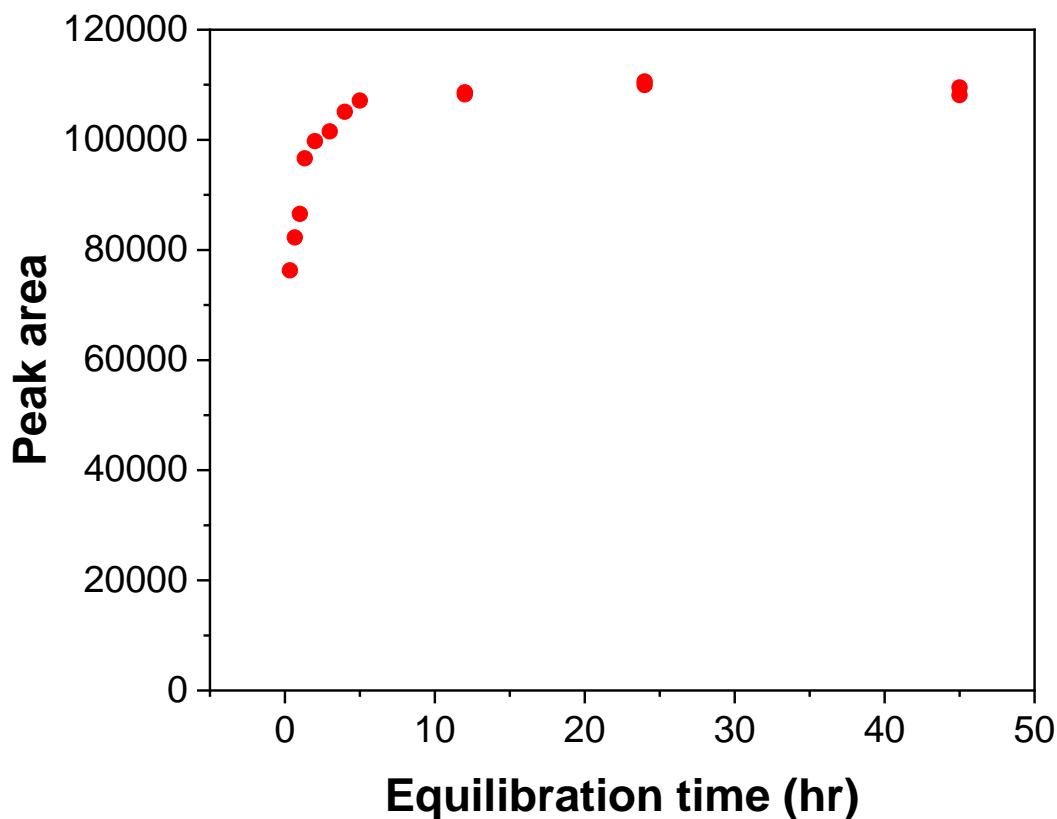


Figure S8. Time-dependence of vapor-liquid equilibrium for electrolyte headspace tests. Samples are pure water.

## 2. *Sampling & detection*

After samples were sufficiently equilibrated, they were submitted to the Agilent 7697A headspace unit carousel for auto-sampling. A pure water sample was included prior to every electrolyte sample (i.e. pure water vial 1 → sample 1 → pure water vial 2 → sample 2 → pure water vial 3 → ...), and electrolyte vials within each set were sampled in a randomized order, specified by an online random number generator. Once a vial cap was pierced, the sample was considered no longer usable (i.e., no vials were double-sampled).

The trajectory of each sample, including temperatures of components, was as follows:

1. On its turn, the sample vial was inserted into the oven of the headspace sampling unit, which did not have an active setpoint and measured  $T \sim 24\text{-}26\text{ }^{\circ}\text{C}$  during tests. Vial remained in the oven for 9 seconds prior to sampling.

## Supplementary Information

- The headspace autosampler needle punctured the vial cap and began pressurizing the sample with helium, the carrier gas. The injection duration was set to 30 seconds.
- The He-carried sample was withdrawn into a sample loop, which was kept at the lowest possible set point of 35 °C.
- The sample was sent through a heated transfer line leading from the headspace unit to the GC. The transfer line was heated at 50 °C.
- The sample entered the GC at the Front Inlet, which was held at 280 °C.
- The sample passed through an Agilent DB-624UI column (30 m length, 0.32 mm diameter, 1.80  $\mu$ ) with the following temperature profile:
  - 1-minute hold at 35 °C
  - 4-minute ramp at 20 °C/min to final temp of 115 °C
  - 1-minute hold at 115 °C
- The sample was finally detected at an Agilent 7890A Thermal Conductivity Detector (TCD).

Following sample processing, TCD results were plotted and water peaks integrated. The peak area of the pure water reference prior to each sample was used as the standard for activity = 1. That is, this area was the denominator in the calculation:

$$a_{water,sample} = \frac{A_{water\ peak,sample}}{A_{water\ peak,reference}}$$

where  $a$  represents species activity and  $A$  represents peak area. The following is a representative TCD spectrum for a blended electrolyte sample.

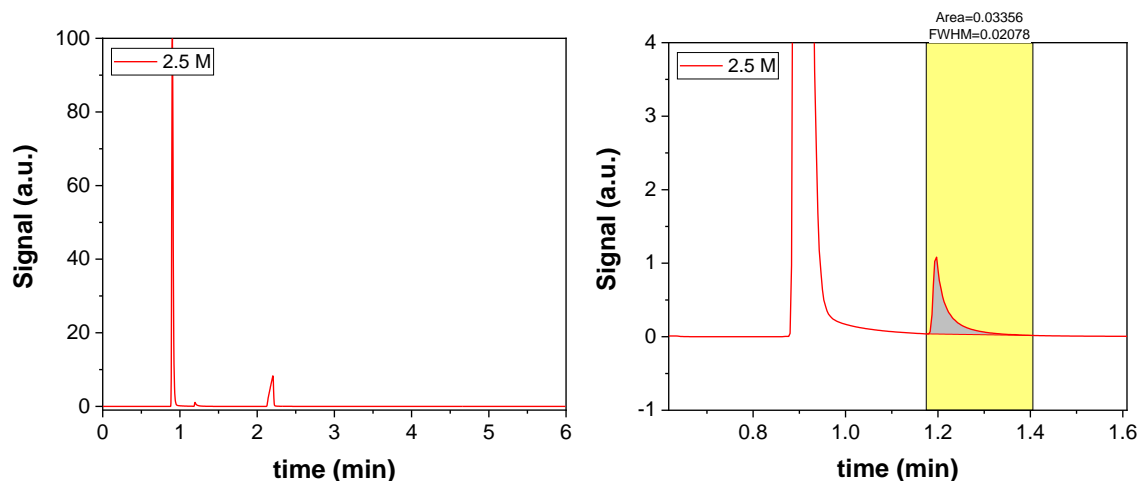


Figure S9. Full and zoomed-in TCD spectra for a representative headspace sample of 2.5 M water in ACN with 0.778 M TBABF<sub>4</sub> and 0.022 M TBAOH. The first peak (~0.9 min) is air; the second, small peak (~1.2 min) is water; and the final peak (~2.1 min) is acetonitrile.

## Supplementary Information

This method for determining activities was validated using a binary ethanol (EtOH) / isopropanol (IPA) system of varying compositions. The activity coefficient of each species in this mixture is predicted to deviate minimally from unity – up to about  $\gamma_{\text{IPA}} = 1.015$  for dilute IPA and  $\gamma_{\text{EtOH}} = 1.013$  for dilute EtOH (using PSRK). That is, the relationship between mole fraction and activity should be roughly a straight line for each species, exhibiting ideality in the Raoult's Law sense. This was observed experimentally, suggesting the quantification method itself does not interfere with the activity measurements. (Figure S10)

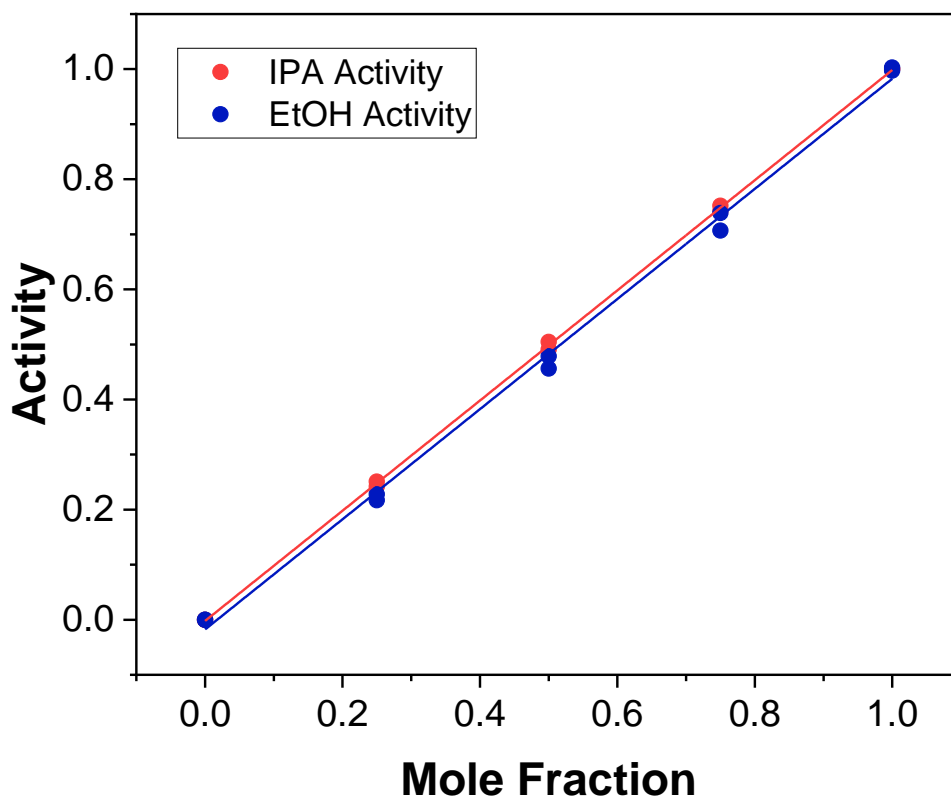


Figure S10. Measured activity-concentration relationship for a binary mixture of ethanol (blue) and isopropanol (red).

### Methods: Linear regression

Most of the linear regression performed in this work was carried out in Origin 2018b. Y-errors were incorporated into the fits in this software where applicable. Instrumental weighting was used for errors, and error was scaled with  $\sqrt{\text{reduced chi-squared}}$ . Fit parameters are reported with 95% confidence intervals.

Specifically for data containing both x- and y-errors, namely the water dependence data from main text Figure 2C, a Matlab script by Wiens employing the methods of York et al. was utilized.<sup>5,6</sup>

## Raw data from main-text figures

Fig 2A: Water concentration-activity relationship for HER electrolyte

Water Concentration (M)	Activity 1	Activity 2	Activity 3	Avg Activity
0	0	0	0	0
0.5	0.12622	0.12193	0.09097	0.11304 ± 0.01570
1	0.26031	0.18365	0.27076	0.23824 ± 0.03884
2.5	0.61005	0.42509	0.57317	0.53610 ± 0.07993
5	0.77496	0.5697	0.64987	0.66484 ± 0.08446
6.6	0.86044	0.87173	0.72846	0.82021 ± 0.06504
8.2	0.99346	0.94075	0.99195	0.97539 ± 0.02450
55.5	1	1	1	1

Fig 2C: Water dependence of HER at -1.875 V vs. Me<sub>10</sub>-Fc

Concentration H <sub>2</sub> O (M)	log (C <sub>H2O</sub> / M)	Activity H <sub>2</sub> O	log (a <sub>H2O</sub> )	Error in log (a <sub>H2O</sub> )	Current density / mA cm <sup>-2</sup>	log (Current density / mA cm <sup>-2</sup> )	Error in log (i / mA cm <sup>-2</sup> )
0.5	-0.30103	0.11304	-0.94677	-: -0.065 +: 0.056	-3.60E-01	-0.44399	-: -0.009 +: 0.009
1	0	0.23824	-0.62299	-: -0.077 +: 0.066	-2.32E+00	0.36495	-: -0.011 +: 0.010
2.5	0.39794	0.5361	-0.27075	-: -0.07 +: 0.060	-1.77E+01	1.24868	-: -0.023 +: 0.014
5	0.69897	0.66484	-0.17728	-: -0.059 +: 0.052	-5.06E+01	1.70408	-: -0.009 +: 0.007
6.6	0.819544	0.82021	-0.08607	-: -0.036 +: 0.033	-6.43E+01	1.80819	-: 0.001 +: 0.005

Note: the 0.5 M data point of this data set was not fit in Figure 2C because the measured partial current was determined to be too low to yield a reliable measure for HER.

See below for more details on error estimation.

Fig 4A: Water concentration-activity relationship for epoxidation electrolyte

Water Concentration (M)	Activity 1	Activity 2	Activity 3	Avg Activity
0	0	0	0	0
0.5	0.18532	0.18596	0.1971	0.18946 ± 0.00541
1	0.28558	0.31913	0.31963	0.30811 ± 0.01593
2	0.49606	0.54726	0.52185	0.52172 ± 0.02090
5	0.79107	0.85994	0.86597	0.83899 ± 0.03398
10	0.92543	0.9786	0.97072	0.95825 ± 0.02343
12.5	0.91607	0.95618	0.95348	0.94191 ± 0.01830
15	0.94637	0.99434	1.02212	0.98761 ± 0.03129
55.5	1	1	1	1

Supplementary Information

Fig 4B: Water concentration-activity relationship for lactonization electrolyte

Water Concentration (M)	Activity 1	Activity 2	Activity 3	Avg Activity
0	0	0	0	0
0.5	0.15441	0.15101	0.15518	0.15353 ± 0.00181
0.7	0.19631	0.20098	0.20607	0.20112 ± 0.00399
1	0.25538	0.3077	0.25893	0.27400 ± 0.02387
1.5	0.35674	0.3458	0.42429	0.37561 ± 0.03471
2	0.41419	0.41277	0.53932	0.45543 ± 0.05932
5	0.61013	0.78799	0.58197	0.66003 ± 0.09121
10	0.88726	1.01342	0.99859	0.96642 ± 0.05630
55.5	1	1	1	1

Fig 4C: Water dependence of cyclooctene epoxidation at 1.45 V vs. Fc

Concentration H <sub>2</sub> O (M)	log (C <sub>H<sub>2</sub>O</sub> / M)	Activity H <sub>2</sub> O	log (a <sub>H<sub>2</sub>O</sub> )	log (Current density / A cm <sup>-2</sup> )	Error in log (i / A cm <sup>-2</sup> )
0.5	-0.30103	0.18946	-0.72248	-3.30549	0.16001
1	0	0.30811	-0.51129	-3.00145	0.01172
2	0.30103	0.52172	-0.28256	-2.70984	0.05482
5	0.69897	0.83899	-0.07624	-2.50142	0.0334
10	1	0.95825	-0.01852	-2.62897	0.04864
12.5	1.09691	0.94191	-0.02599	-2.64739	0.03956
15	1.17609	0.98761	-0.00541	-2.73304	0.08898

Fig 4D: Water dependence of cyclohexanone lactonization

Concentration H <sub>2</sub> O (M)	log (C <sub>H<sub>2</sub>O</sub> / M)	Activity H <sub>2</sub> O	log (a <sub>H<sub>2</sub>O</sub> )	log (Current density / A cm <sup>-2</sup> )
0.5	-0.30103	0.15353	-0.8138	-3.50516
0.7	-0.1549	0.20112	-0.69654	-3.27263
1	0	0.27400	-0.56224	-3.0002
1.5	0.17609	0.37561	-0.42526	-2.85696
2	0.30103	0.45543	-0.34158	-2.59061
2	0.30103	0.45543	-0.34158	-2.69673
5	0.69897	0.66003	-0.18044	-2.49055
10	1	0.96642	-0.01483	-2.45865
10	1	0.96642	-0.01483	-2.45347

**Discussion: Measured activity curves overlaid on one another**

In order to compare the behavior of water in the blended electrolyte at varying TBABF<sub>4</sub> contents, activity measurements from the various electrolytes reported here – 800 mM TBABF<sub>4</sub>, 350 mM TBABF<sub>4</sub> + 400 mM cyclohexanone, ~100 mM TBABF<sub>4</sub> + 200 mM cyclooctene, as well as the binary water/acetonitrile mixture (0 mM TBABF<sub>4</sub>) – were overlaid on the same plot. (Figure S11) Note that for the purposes of this analysis, we will ignore the small amount of organic substrate in the 350 mM and 100 mM TBABF<sub>4</sub> samples; however, a more complete comparison could be drawn by removing these substrates.

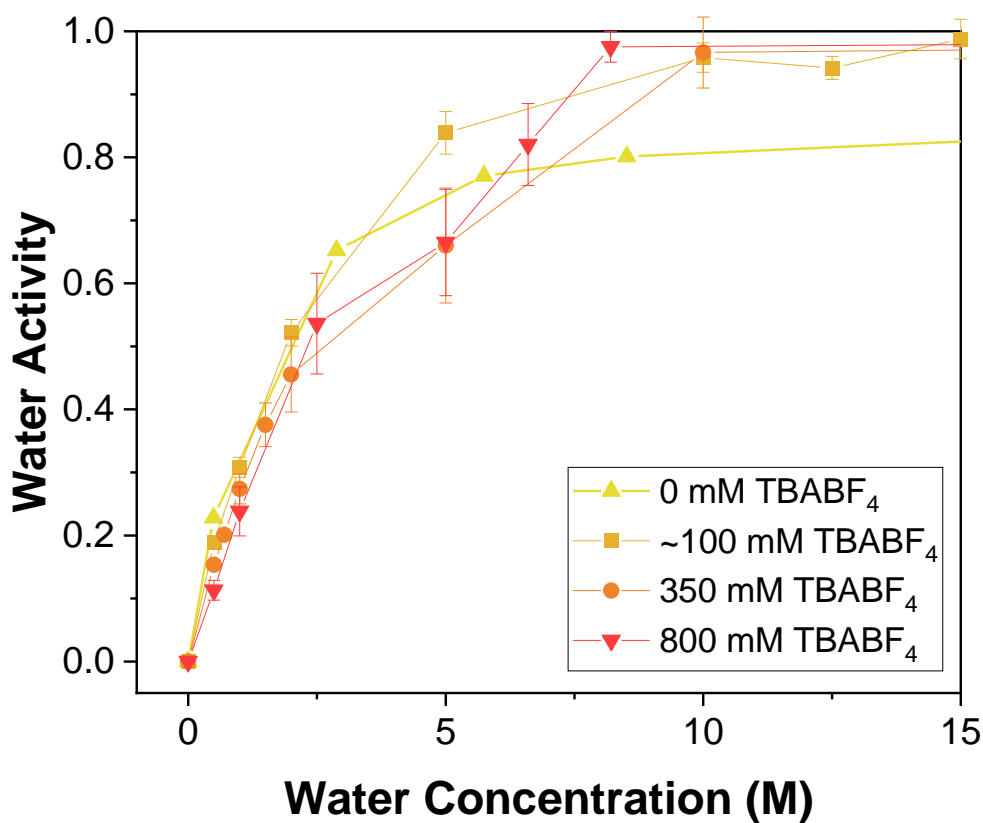


Figure S11. Overlay of four data sets: binary water/acetonitrile as reported in literature<sup>7,8</sup> (yellow), acetonitrile/water + ~100 mM TBABF<sub>4</sub> + 200 mM cyclooctene (light orange), acetonitrile/water + 350 mM TBABF<sub>4</sub> + 400 mM cyclohexanone (dark orange), and acetonitrile/water + 800 mM TBABF<sub>4</sub> (red).

As mentioned in the main text, the activity of water reaches unity at much lower concentrations for higher TBABF<sub>4</sub> content. This is because unfavorable interactions with the highly hydrophobic TBA<sup>+</sup> cation increase water activity, leading to phase separation at lower water concentrations with increasing TBA<sup>+</sup> content. However, there is a markedly different trend at lower water concentrations. Zooming in... (Figure S12)

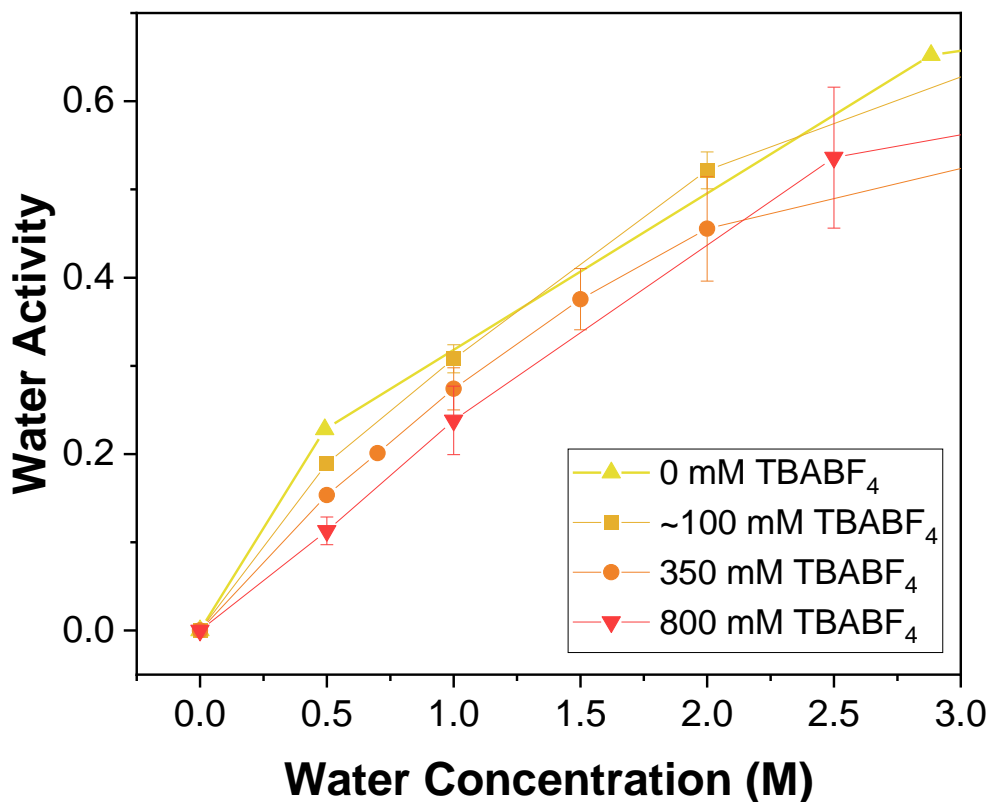


Figure S12. Zoomed-in water concentration-activity relationships in acetonitrile with varying TBABF<sub>4</sub> content.

We can observe that at low water concentrations, the trend reverses: water activity at a given concentration of water is measured to be higher at lower concentrations of TBABF<sub>4</sub>. This could be due to a number of factors: for instance, perhaps favorable interactions with the BF<sub>4</sub><sup>-</sup> ion stabilize water at these low concentrations. Perhaps trace halogens or other salt impurities in the TBABF<sub>4</sub> play a larger role in coordinating water at these low concentrations. These are hypotheses we will seek to test in future work.

### Discussion: Faradaic efficiency of HER

Due to the incomplete sealing of the H-cell setup used in experiments, it was not possible to quantify HER during most of the electrochemical tests reported here. However, constant-potential holds in sandwich cell setups connected to a gas chromatograph confirm 100% Faradaic efficiency (FE) for HER at moderate currents (~0.1 – 10 mA). This is corroborated by results detailed in previous O-atom transfer works.<sup>9,10</sup>

## Supplementary Information

The primary difference between the system used for FE closure analysis and the system used for kinetic analysis in this work, in terms of variables that may affect FE, is that the kinetic analysis setup cannot be fully sealed. Because the tests are not conducted in a glovebox, glovebag, or other rigorously controlled atmosphere outside of the cell, it is necessary to purge an inert gas through the working compartment in order to remove dissolved O<sub>2</sub>. When O<sub>2</sub> is present, background ORR current artificially inflates the measured current by a small amount (~0.2 mA). Further discussion on how this current was controlled and eliminated can be found below. (See Discussion: Experimental troubleshooting & minimizing background current.)

### Reference: Volmer, Tafel, and Heyrovsky steps

The most common named microkinetic reaction steps in the HER/HOR couple reaction pathway are as follows (shown here in the alkaline case):



### Discussion: TST reaction rate expression formulation

Here we will explain the derivation of the rate expression for a reaction based on Transition State Theory – motivating our use of the term “activity” in the discussion, rather than “chemical potential,” despite the fact that these two quantities are directly related. Many thanks to Thejas Wesley for contributing the following distinction.

To begin, we write classical transition state theory rate expressions for an arbitrary elementary surface reaction – noting of course that this would also apply to reactions not taking place at surfaces, just with different notation:



$$r = \frac{k_B T}{h} \theta_{\ddagger} \quad (\text{Eq. 1})$$

$$K_{eq}^{\ddagger} = \exp\left(\frac{-\Delta G^{0\ddagger}}{RT}\right) = \frac{\gamma_{\ddagger} \theta_{\ddagger}}{\prod_j a_j^{v_j}}$$

$$\Rightarrow \theta_{\ddagger}(\{a_j\}) = \exp\left(\frac{-\Delta G^{0\ddagger}}{RT}\right) \frac{1}{\gamma_{\ddagger}} \prod_j a_j^{v_j} \quad (\text{Eq. 2})$$

where  $\{v_j\} = \{\alpha, \beta, \dots\} > 0$  are (absolute value) stoichiometric coefficients of reactants  $\{A, B, \dots\}$  moving into the transition state,  $a_j$  is the thermodynamic activity of species  $j$ ,  $\gamma_{\ddagger}$  is the activity coefficient of the adsorbed transition state, and  $\Delta G^{0\ddagger}$  is the *standard state* activation free energy:

## Supplementary Information

$$\Delta G^{0\ddagger} = \mu_{\ddagger}^0 - \sum_j \nu_j \mu_j^0$$

where  $\mu_j^0$  is the standard state chemical potential of species  $j$ .

Bringing the product into the exponential,

$$\Rightarrow \theta_{\ddagger}(\{a_j\}) = \exp\left(\frac{-\Delta G^{0\ddagger} + RT \sum_j \nu_j \ln a_j}{RT}\right) \frac{1}{\gamma_{\ddagger}}$$

we can then substitute for  $\Delta G^{0\ddagger}$  using the expression above,

$$\theta_{\ddagger}(\{a_j\}) = \exp\left(\frac{-(\mu_{\ddagger}^0 - \sum_j \nu_j \mu_j^0) + RT \sum_j \nu_j \ln a_j}{RT}\right) \frac{1}{\gamma_{\ddagger}}$$

and from here we can combine the sums,

$$\theta_{\ddagger}(\{a_j\}) = \exp\left(\frac{-[\mu_{\ddagger}^0 - \sum_j \nu_j (\mu_j^0 + RT \ln a_j)]}{RT}\right) \frac{1}{\gamma_{\ddagger}}$$

at which point we recognize a common definition for chemical potential:  $\mu_j = \mu_j^0 + RT \ln a_j$ . Substituting this in the expression, we get

$$\theta_{\ddagger}(\{\mu_j\}) = \exp\left(\frac{-[\mu_{\ddagger}^0 - \sum_j \nu_j \mu_j]}{RT}\right) \frac{1}{\gamma_{\ddagger}}$$

And finally, we combine the numerator in the exponential into  $\Delta G^{\ddagger} = \mu_{\ddagger}^0 - \sum_j \nu_j \mu_j$ , which is the free energy change going from the actual solution species to the (standard state of the) transition state:

$$\theta_{\ddagger}(\{\mu_j\}) = \exp\left(\frac{-\Delta G^{\ddagger}}{RT}\right) \frac{1}{\gamma_{\ddagger}} \quad (\text{Eq. 3})$$

Combining Eq. 1 and 2, the rate may be written as:

$$r = \frac{k_B T}{h} \theta_{\ddagger} = \frac{k_B T}{h} \exp\left(\frac{-\Delta G^{0\ddagger}}{RT}\right) \frac{1}{\gamma_{\ddagger}} \prod_j a_j^{\nu_j} = r(\{a_j\}) \quad (\text{Eq. 4})$$

But instead combining Eq. 1 and 3, it may instead be equivalently written as

$$r = \frac{k_B T}{h} \theta_{\ddagger} = \frac{k_B T}{h} \exp\left(\frac{-\Delta G^{\ddagger}}{RT}\right) \frac{1}{\gamma_{\ddagger}} = r(\{\mu_j\}) \quad (\text{Eq. 5})$$

Eq. 4 and 5 are identical, but simply in different notation: using the activity form (Eq. 4) implies that the free energy used in the rate constant is based on the chemical potential of the fluid species at the standard state; however, using (Eq. 5) implies that the free energy used in the rate constant is based on the chemical potential of the fluid species at the real concentrations/partial pressures in the reactor.

Eq. 4 is the more familiar formalism, common throughout thermal catalysis literature, and which we employ in the context of this work. This is why we use the term “activity” rather than “chemical potential” throughout the main text.

*A note on “hot” reactants and other thermodynamic exceptions*

While in this instance we hold activity to be the best descriptor of reaction rate, there are cases in which reacting species’ thermodynamic activities are not always the best descriptors of reaction rate. An example discussed in the main text is the previously-reported “fortuitous cancellation” of activity coefficients of the reactant and transition state species.<sup>11</sup> In this case the best variable for describing reaction rate comes out to be reactant concentration rather than activity. Similarly, reactions which are “activationless” or “barrierless”<sup>12</sup> – in certain cases, involving species so reactive that they instantly react upon collision with essentially 100% probability – may be limited by collisions and therefore also dependent upon reactant concentration. Another example of activity not being the best descriptor is in the literature of “hot” reactants – that is to say, species which react while they are not yet at thermodynamic equilibrium with the surface.<sup>13</sup> Reactants impinging upon a surface or entering from the subsurface carry with them energy – in many cases, translational energy – that has not yet been dissipated as the species come into equilibrium with the surface at hand. This extra energy can be used to overcome activation barriers, thereby yielding different reaction rates than might be expected from the thermodynamics of the reactants and surface alone. In these senses, reactant activity is not always a good descriptor of rate.

### Discussion: HER on Pt cathode

In addition to the HER experiments reported in the main text, we also conducted HER on a Pt cathode, in accordance with the methods reported above (see Methods: Preparation of RDE working electrodes: 2. Platinum disk<sup>4</sup>). The results of these experiments are shown below. (Figure S13)

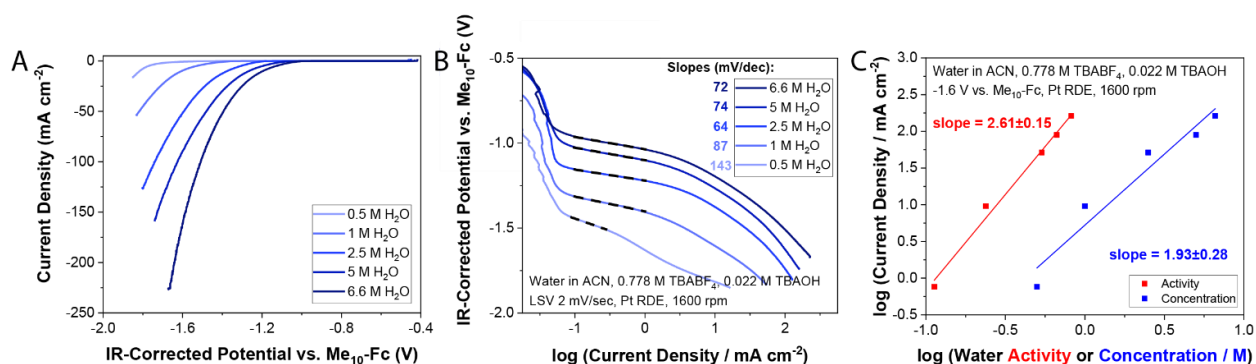


Figure S13. HER on Pt at various concentrations of water in acetonitrile + 0.778 M TBABF<sub>4</sub> + 0.022 M TBAOH. A) Raw LSV data plotted vs. Me<sub>10</sub>-Fc. B) The same data visualized on a Tafel plot. C) Water dependence of HER on Pt at a -1.6 V vs. Me<sub>10</sub>-Fc.

As expected, Pt catalyzes HER in the blended electrolyte at much less reductive potentials than required by Au for similar rates. In addition, once onset occurs, the Tafel slope is lower for Pt than

for Au, meaning the current responds more strongly to applied voltage. It may be noted that the reported Tafel slopes increase with decreasing concentrations of water, similar to what was noted in the main text. From 6.6 M water down to 2.5 M water, the measured Tafel slope is between 64-74 mV/dec, which is consistent with a RDS in which no ET is involved, but rather there is a pre-equilibrated ET step. (see Reference: Tafel slopes) At 1 M water, the Tafel slope increases to 87, and at 0.5 M water, the slope increases further to 143 mV/dec. There could be a variety of factors leading to an increase in Tafel slope across this range, similar to the increase reported in the main text – however, because the swing in slopes is so large that it could be partially attributed to a changing mechanism (i.e. cardinal “60 mV/dec” slope  $\rightarrow$  cardinal “120 mV/dec” slope), we elected to focus instead on results obtained on Au, where the direct mechanism is less likely to be changing as conditions are altered.

It is notable, however, that water dependences in the case of both Au and Pt (with potentials referenced to Me<sub>10</sub>-Fc) are measured to be between 2.5-3. This may suggest that the measured water order in fact has little to do with surface catalytic phenomena at all.

### Reference: Tafel slopes

As a reminder, the general form taken by a Tafel slope at standard conditions is:

$$m_T = \frac{59 \text{ mV/dec}}{n + \beta q}$$

where  $m_T$  is the Tafel slope,  $n$  is the number of electrons transferred prior to the RDS,  $q$  is the number of electrons transferred during the RDS, and  $\beta$  is the symmetry factor, often assumed to be 0.5. This latter assumption is supported by historical measurements of acidic HER kinetics on Pt,<sup>14</sup> although the symmetry factor (or at least the transfer coefficient  $\alpha$  as the experimentally measurable parameter) can change with electrolyte composition,<sup>15</sup> and apparent  $\beta$  from literature measurements on Au<sup>16</sup> can be calculated to be anywhere between 0.37-0.57. Assuming  $\beta$  is 0.5, some examples of cardinal values of Tafel slopes would be:

- 120 mV/dec:  $n = 0, q = 1, \beta = 0.5$  (initial electron transfer RDS)
  - e.g., the Volmer step
- 60 mV/dec:  $n = 1, q = 0$  (subsequent chemical step RDS)
- 40 mV/dec:  $n = 1, q = 1, \beta = 0.5$  (second electron transfer RDS)
  - e.g., the Heyrovsky step
- 30 mV/dec:  $n = 2, q = 0$  (subsequent chemical step RDS)
  - e.g., the Tafel step

As previously reported, these cardinal values can be altered by a wide variety of phenomena in an electrocatalytic system, and are not necessarily expected to be observed in actual measurements.<sup>17</sup>

**Discussion: Confirming lack of transport limitations in RDE measurements**

The lack of limitations due to diffusional mass transport through the electrolyte was confirmed by varying the rotation rate of the RDE during LSV experiments. The Tafel plots for these experiments are shown below. Note that in general there is no monotonic trend in Tafel slope as rotation rate is increased/decreased, and in fact experiments conducted at 900 RPM, 1600 RPM, and 2500 RPM all yield similar Tafel slopes within the same fit region and similar currents at the same potential. These results serve to quell concerns that slow H<sub>2</sub> transport away from the electrode surface in particular leads to lower HER rates.<sup>18</sup>

Supplementary Information

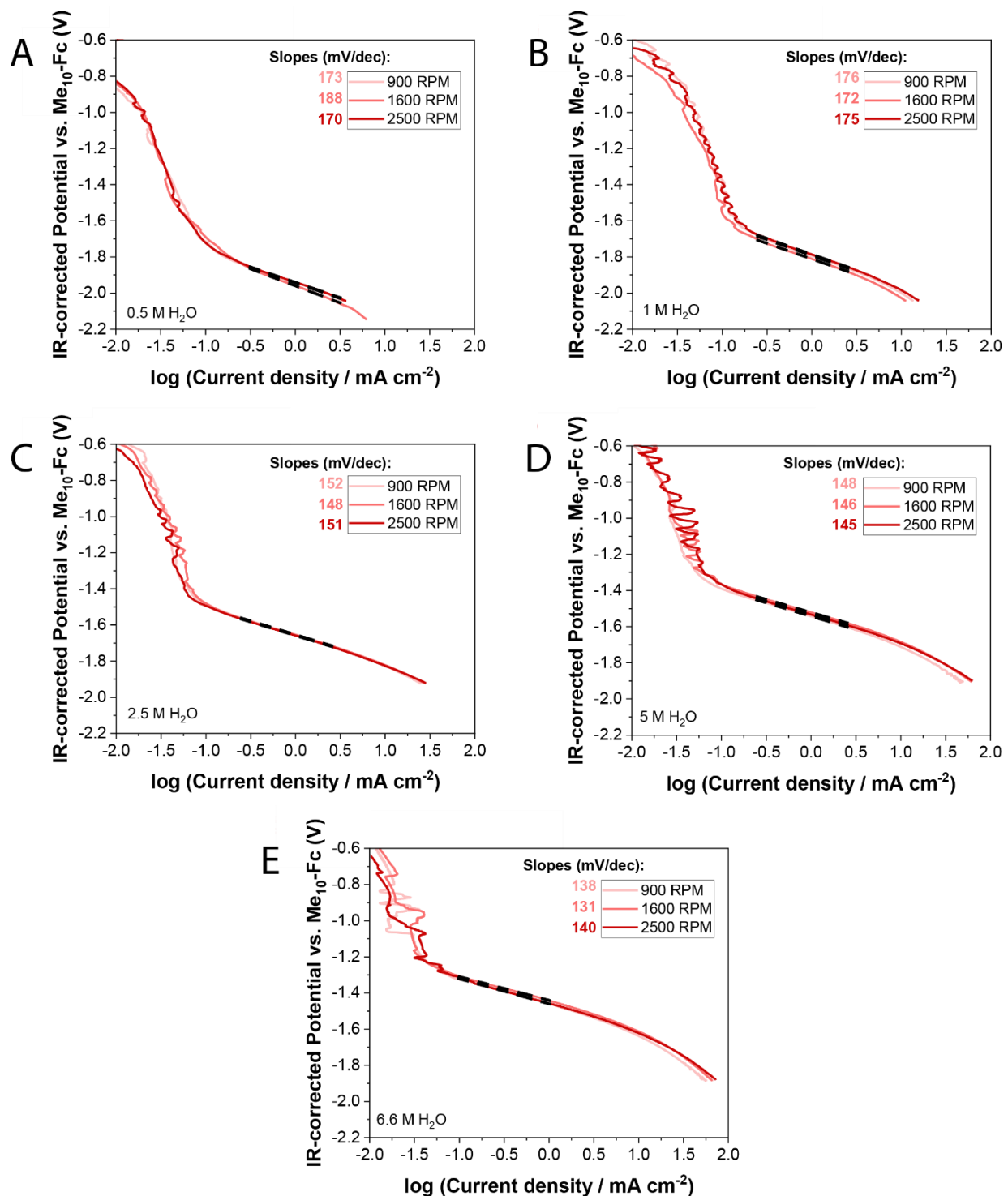


Figure S14. Rotation rate dependences for HER shown via Tafel plots taken at 900, 1600, and 2500 RPM. (Order: 1600 – 900 – 2500.) Electrolytes contained acetonitrile, 0.778 M TBABF<sub>4</sub>, 0.022 M TBAOH, and: A) 0.5 M water, B) 1 M water, C) 2.5 M water, D) 5 M water, and E) 6.6 M water.

**Discussion: ET potential scales versus CPET potential scales (Measurement of RHE in blended electrolyte)**

As mentioned in the main text, the reference potential for reported data is the redox potential of Me<sub>10</sub>-Fc, the oxidation and reduction of which involves only the transfer of electrons to the Fe center. However, because the rate-determining step of HER involves a proton transfer, the energetics of the proton in solution will also impact the reversible potential for HER, which is definitionally the reversible hydrogen electrode, RHE. The thermodynamics of protons in the blended electrolyte are subject to change alongside alterations in water composition. Here we detail our accounting for the changing thermodynamics of proton transfer with blended electrolyte composition through the direct measurement of RHE in those electrolytes.

A method to measure RHE in any electrolyte has been reported in the literature<sup>19</sup> and has also been extended to apply to the determination of the potential of H-atom transfer reactions.<sup>20,21</sup> In short, the method involves measuring the OCV of a clean Pt electrode in the electrolyte of interest versus a pseudoreference electrode while simultaneously flowing H<sub>2</sub> gas to saturate the electrolyte. As long as the electrolyte contains some reasonably labile proton, HER/HOR is the most facile reaction on a clean Pt surface, having the largest exchange current density  $i_0$ . Because of this, the potential of the Pt electrode is defined by that equilibrium. By subsequently measuring the potential of the pseudoreference electrode versus Fc or Me<sub>10</sub>-Fc, it is then possible to define RHE vs. that ET reference, which can in turn be referenced in electrochemical experiments.

We employed this OCV measurement for the determination of RHE in the blended electrolytes of interest, with some notable changes to procedure. The main difference was in the preparation of the Pt electrode. Rather than H<sub>2</sub> flame-annealing a Pt wire that was then handled under H<sub>2</sub> and/or N<sub>2</sub> atmospheres prior to the experiment, we elected to use the same Pt disk employed in HER experiments and apply the same preparation procedures as for those tests. (see Methods: Preparation of RDE working electrodes: 2. Platinum disk<sup>4</sup>) The reasoning behind this was that it should be much more likely for condensed-phase species such as acetonitrile and tetrabutylammonium to poison the Pt surface than for gas-phase species such as O<sub>2</sub> or trace contaminants in the air to do so – and the Pt must be exposed to the condensed-phase species regardless. Moreover, we have evidence that the preparation procedures employed in this work have been sufficient to observe H<sub>UPD</sub> peaks on cyclic voltammograms of Pt in aqueous electrolytes, and to our understanding, these are more sensitive measurements than the OCV measurements we are attempting here. In order to test this hypothesis that micropolishing + sonication + electro-oxidative treatment in H<sub>2</sub>SO<sub>4</sub> was sufficient to clean the Pt for OCV measurements, we used this preparation procedure and measured the OCV of the Pt versus our pseudoreference in two aqueous solutions: one at pH 1 (0.09167 M H<sub>2</sub>SO<sub>4</sub>), and one at pH 13 (0.1 M KOH). Note the molarity of H<sub>2</sub>SO<sub>4</sub> required for a solution of pH = 1 was calculated by assuming full dissociation of the first proton and a pK<sub>a,2</sub> of 2. The results of two representative OCV measurements are shown here.

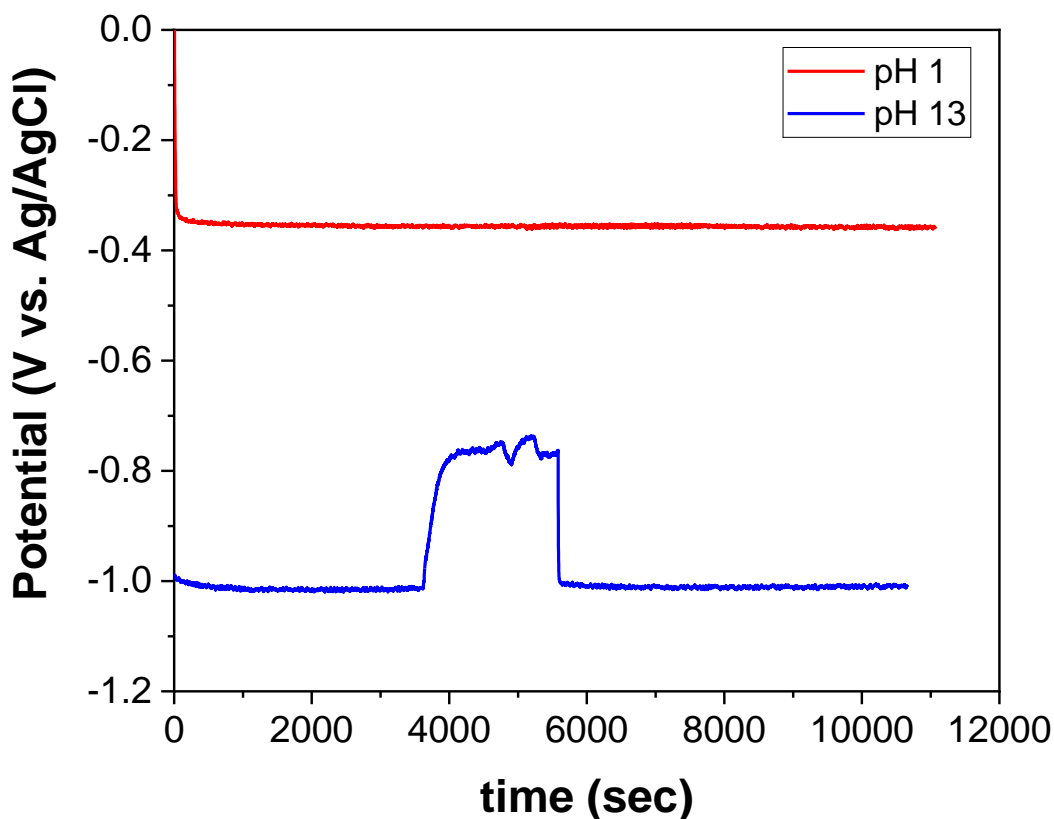


Figure S15. OCV measurements of Pt electrodes versus Ag/AgCl pseudoreference in a pH 1 electrolyte (red) and a pH 13 electrolyte (blue). The bump from  $t = 3600$  sec to  $t = 5580$  sec corresponds to when the working electrode was rotated at 1600 RPM.

During the OCV measurements of the aqueous solutions, we monitored the OCV over the course of about 3 hours. For a majority of this time, the RDE setup was allowed to sit still, not rotating, with a direct H<sub>2</sub> purge of 20 sccm into the working electrolyte and a parafilm seal around the top of the H-cell used for the measurements. However, the effect of rotation was also tested. The RDE was rotated at a rate of 1600 RPM from  $t = 5100$  sec (1.42 hr) to  $t = 7620$  (2.12 hr) in the pH 1 case, and from  $t = 3600$  sec (1 hr) to  $t = 5580$  sec (1.55 hr) in the pH 13 case. From Figure S15, we can see that there was minimal effect of rotation on the measured OCV in the pH 1 case, whereas the measured potential in the pH 13 case increased markedly with working electrode rotation.

The fact that stirring impacted the OCV measurement was at first a bit concerning to us. However, upon closer examination, we noted that other changes to the system could also induce increases in the measured OCV, such as the removal of the loose parafilm seal or the adjustment of the position of the H<sub>2</sub> purge line. We hypothesize that these adjustments actually led to an increase in the dissolved O<sub>2</sub> content, which in turn led the OCV to be defined by a mixed potential involving both

HER/HOR and OER/ORR. This effect was only observed in alkaline conditions because HER/HOR is kinetically more difficult in base than in acid, whereas OER/ORR is relatively more favored kinetically in base than in acid – essentially, the exchange current densities for the two couples became comparable in the alkaline condition. The key, then, was to ensure these measurements fully excluded  $O_2$  to the best of our ability. By running the same OCV measurements in a sandwich cell setup where it was easier to seal against air while purging  $H_2$ , (Figure S16) we determined that the non-stirred condition in the H-cell setup was sufficient for excluding  $O_2$ , as the  $\Delta OCV$  between pH 1 and pH 13 conditions was nearly identical. ( $[OCV_{pH1} - OCV_{pH13}]_{sandwich} = 657.7$  mV, while  $[OCV_{pH1} - OCV_{pH13}]_{Hcell} = 658.7$  mV. Note the theoretical value for this difference is roughly  $(12 \text{ pH}) \cdot (293 \text{ K}/298 \text{ K}) \cdot (59 \text{ mV/pH}) = 696$  mV, implying a reasonable difference in junction potentials  $\Delta V_{junct}$  of about 34-35 mV between acidic and alkaline conditions.

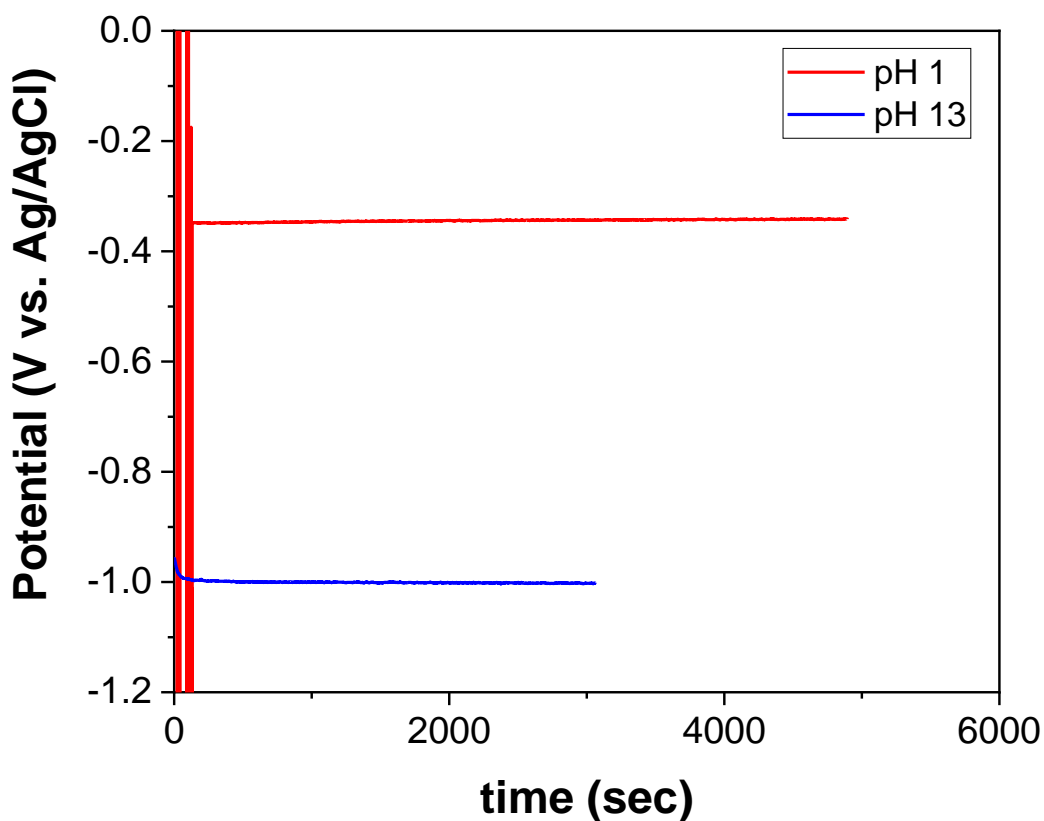


Figure S16. OCV measurements of Pt foil electrode versus Ag/AgCl pseudoreference for the aqueous pH 1 (red) and pH 13 (blue) electrolytes, conducted in a sandwich cell.

With our experimental conditions validated by the aqueous electrolytes, we used this procedure (Pt prep as above for RDE disk, no stirring,  $H_2$  purge) to measure OCVs for the blended electrolytes. For each experiment, the OCV was first measured for at least 4 hours. This was followed by a CV between 0 – -1.5 V vs. the pseudoreference, a short CA at -0.8 V, an LSV from

## Supplementary Information

+0.1 V vs. OCV to roughly -2 V vs. the pseudoreference, and a final OCV, in order to glean information on the overpotentials required for HER on the Pt working electrode and the OCV following a reductive hold. Steps after the first OCV were not strictly necessary. Following this final OCV, the pseudoreference was removed from the cell, quickly rinsed with acetone and water, transferred to a new sandwich cell, and immediately calibrated versus Fc in an electrolyte of composition corresponding to that of the OCV measurement. Results are shown below.

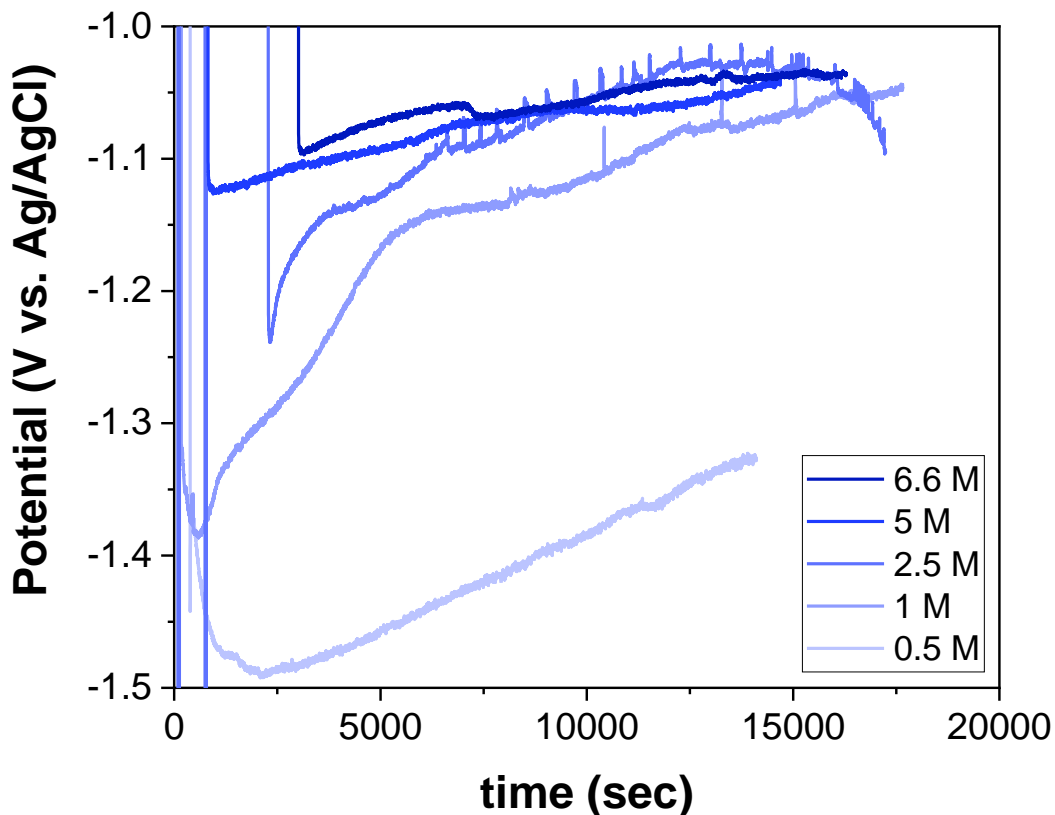


Figure S17. OCV measurements in the various blended electrolyte compositions reported in this work. Darker blue corresponds to higher water content.

Figure S17 displays the OCV measurements in each electrolyte composition over time. It can be seen that the measurement drifts, without an obvious plateau of steady potential, over the course of the 4+ hours. Moreover, the drift happens at different rates for different water content.

Following the voltammograms, which did not yield substantially more information beyond the relatively low overpotentials required for HER/HOR on the Pt electrode, final OCV measurements of various durations were conducted. These results are shown below.

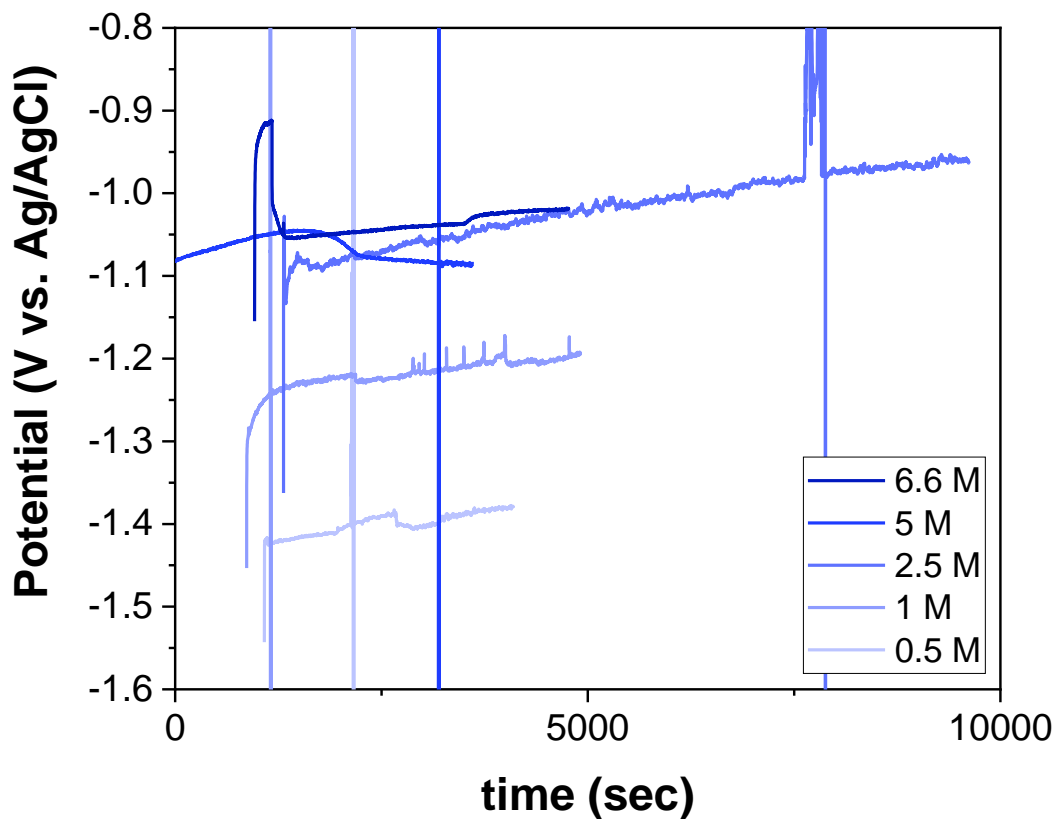


Figure S18. The final OCV measurements prior to calibration of the pseudo-reference. During the final OCVs, potentials continued to drift at similar rates as in the initial OCV measurements.

Following the OCV measurement procedure, the pseudoreference electrode was calibrated versus Fc, which was added to a few mL of the electrolyte that had previously been set aside. Fc calibrations are shown below.

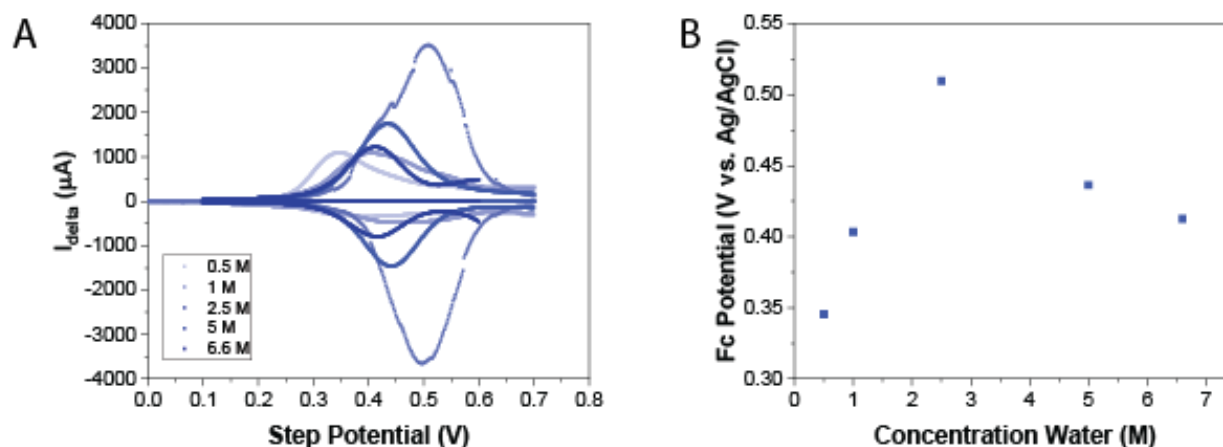


Figure S19. Fc calibrations of the pseudo-reference electrode following OCV measurements. A) Raw SWV data. B) Resulting averages of oxidative and reductive peak potentials. Only the first SWV was used in every case.

It should be noted that in contrast to the Fc calibrations used for HER experiments, these calibrations were conducted after the pseudoreference had been allowed to equilibrate in the electrolyte of interest for many hours. It is perhaps for this reason that there was not an overall trend to the measured potential of the pseudoreference versus Fc. In fact, it seems that there is more of a correlation between duration of the OCV procedure and potential of the pseudoreference versus Fc than anything else, with the longest-duration experiment being the one at 2.5 M water, and the shortest being 0.5 M water. That is, longer equilibration with the blended electrolyte leads to a decreasing potential of the pseudoreference. This would be observed as both an increase in the measured OCV over time, as well as an increase in the measured potential of Fc over time.

#### *Water dependence at a constant V vs. RHE*

Because there is no plateau in the OCV data – no clear stopping point for the experiment – we are left with a variety of reasonable approaches we could take in order to process the data. A non-comprehensive list of these approaches, as well as reasoning behind each approach, follows here:

1. Compare all OCVs at a consistent time point within the respective measurement

In this approach, we treat all data at a consistent time point in the experiment as being equivalent. This might be justified by the fact that for each experiment, the pseudoreference electrode starts in roughly the same condition. In addition, in the LSV data set, comparable data is taken at comparable time points in the experiment, lending another reason in favor of this approach. However, taking this approach requires that we further ask: at what point is it reasonable to compare data? This added layer of choice is consequential, as the rate of OCV drift is inconsistent between tests.

2. Compare OCVs once drift rate over time becomes comparable

## Supplementary Information

Because this drift rate in OCVs does change over time and is not consistent, we could also elect to take each trace's OCV once the drift rate has become more internally consistent. Put another way, this approach would be to wait until the derivative of the OCV with respect to time becomes roughly constant, and measure the OCV at this point. There is not a strong physical basis for such an approach, however.

### 3. Measure OCVs from the initial "dip"

An interesting feature of each of these data sets is the initial OCV "dip" that occurs sometime within the first hour of the experiment. Because we do not saturate the electrolyte with H<sub>2</sub> prior to the start of the experiment, we hypothesize that this dip is attributable to the point at which H<sub>2</sub> has displaced enough O<sub>2</sub> from the air that the dominant reaction defining the potential of the electrode switches from OER/ORR to HER/HOR. We could elect to take the approach of measuring OCVs from this initial dip, perhaps with the motivation that changes in the potential over time are due to changes in the electrolyte; however, we do not believe this is the case, and there is nothing particularly special about the point in time where the dip occurs from the perspective of the pseudoreference electrode.

### 4. Extrapolate long-time data back to the origin

If we wished to capture the behavior of the reference at the beginning of the experiment, one approach might be to extrapolate the data from the constant-drift-rate region of the OCV profile back to the origin. This approach assumes both that the reference behavior at the beginning of the experiment is most relevant, and also that deviations from the constant-drift-rate changes in the electrolyte should be ignored, neither of which are based on convincing physical arguments.

### 5. Take only the OCV value measured at the very end of the run

Finally, we could also assume that all transient changes observed in the OCV data are entirely attributable to changes in the pseudoreference over time, and that the point at which the measured OCV most closely reflects the potential which can be related to the Fc calibration is the OCV measured immediately prior to that calibration. We find this to be a reasonable hypothesis, and likely the closest to the truth. The only issue is that we do not know how the behavior of the reference changes as it is moved from one cell to another and rinsed with water and acetone. It is possible that this part of the procedure "resets" the pseudoreference electrode in some way, in which case the data collected here may not mean much. We have yet to perform experiments without washing the pseudoreference.

In truth, it is difficult to know which of these approaches will yield the most accurate results. We visualize below how each approach leads to a different interpretation of the water dependence data.

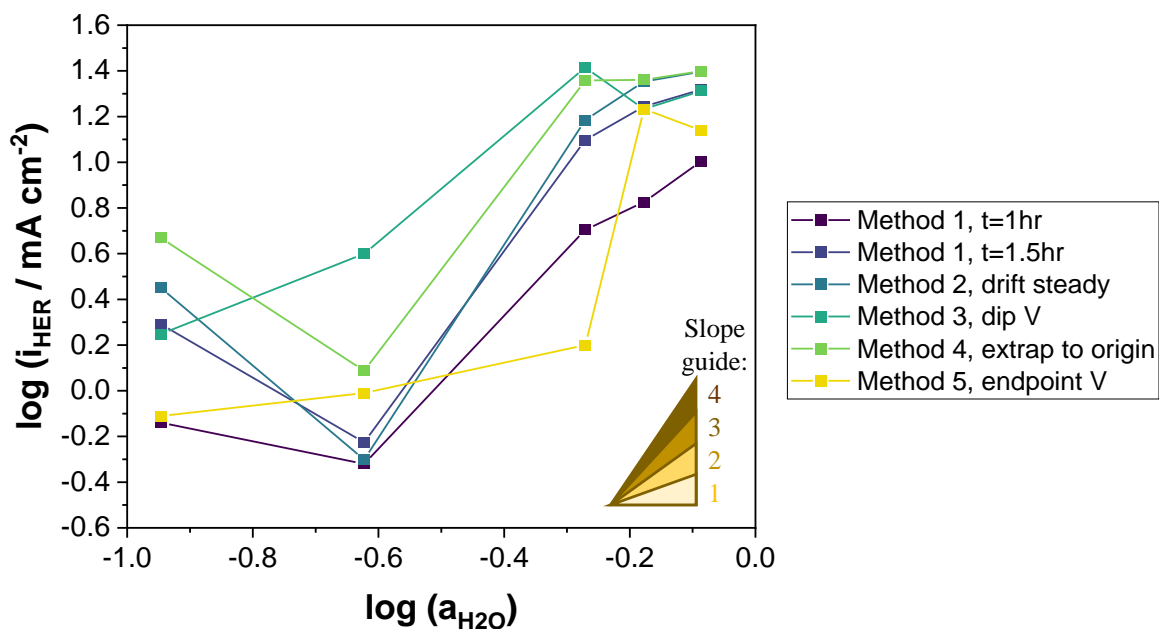


Figure S20. Water dependence data at a constant potential vs. RHE, using various approaches to quantify RHE. Slope inset is provided as a visual reference.

From these various approaches, it seems that there is still a strong dependence of HER rate on water content. However, the sign and magnitude of that dependence is particularly unclear at low water activity. Between the 0.5 M water and 1 M water samples, the various methods for determining RHE yield water dependences ranging from 1.1-order all the way down to -2.3-order. On the other hand, between the 1 M and 2.5 M water samples, point-to-point slopes range from 0.6 to 4.2. In general, the various approaches seem to indicate a low dependence on water in the low-activity limit, and a dependence on water that is on-par with the dependence reported in the main text for all other data points (1.4-3.4). In the specific case of approach #5, the endpoint OCV method which we find the most compelling, the water dependence appears to exhibit more of a step-change behavior: low dependence between 0.5 M – 2.5 M, low dependence between 5 M – 6.6 M, but an increase of about an order of magnitude in HER current between 2.5 M and 5 M water.

It is partly due to a combination of the many uncertainties in this RHE measurement that we elected to instead analyze water dependence at a constant potential versus an ET reference. In addition, knowing potentials versus the ET reference in the case of HER in the blended electrolyte is also practically useful in the sense that the full cell voltage may be better understood in this frame of reference – assuming the counter reaction is also understood w.r.t. an ET potential scale.

**Discussion: pH effect on HER**

Experiments were carried out in order to assess the impact of adding explicit base to the electrolyte in the form of TBAOH. Because the experiment with no TBAOH was unbuffered, it was subject to unmitigated pH changes during the LSV. These tests served to very roughly probe whether the interfacial pH in neutral tests was substantially different from a bulk alkaline experiment. This is of relevance since some electrochemical systems operate with no buffer, but only water in acetonitrile with TBABF<sub>4</sub> and similar aprotic salts.

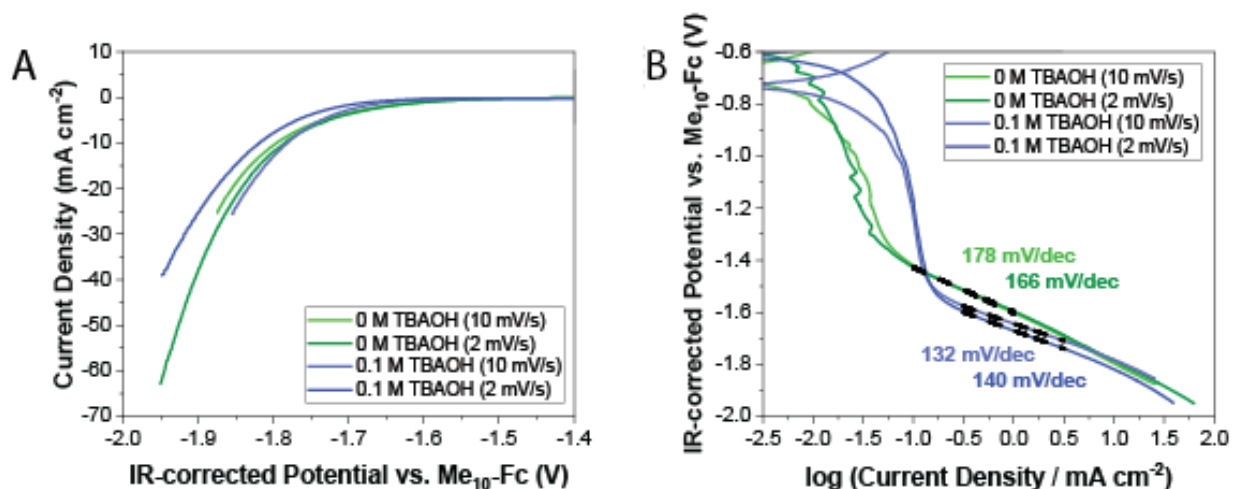


Figure S21. LSVs of electrolyte solutions containing 2.5 M water with either 0 M TBAOH/0.8 M TBABF<sub>4</sub> (green) or 0.1 M TBAOH/0.7 M TBABF<sub>4</sub> (blue). A) Raw LSV data and B) the same data presented as a Tafel plot.

Note that while the scan rates were different between the light and dark blue data points, as well as between the light and dark green data, the main point being illustrated is that run-to-run differences are comparable to differences brought about due to explicit base, especially at higher currents ( $>10$  mA/cm<sup>2</sup>). From these results we can see that the initial takeoff of HER may be slightly delayed in the alkaline case relative to the neutral case, which may be expected from a thermodynamic perspective – in fact, a pH shift of this magnitude should theoretically yield a larger potential gap than observed,  $\sim 350$  mV. However, these differences roughly cancel out once currents reach  $>10$  mA/cm<sup>2</sup>. Under these conditions HER is producing enough base at the electrode surface that the reaction environment in the neutral case is essentially similar to that in the alkaline case. Note that the Tafel slope, however, is fit at lower current densities and is therefore sensitive to the bulk pH value – with lower Tafel slopes attainable under more alkaline conditions.

**Discussion: Experimental troubleshooting & minimizing background current**

As this project was taking shape, we progressed through several stages of experimental setups. These are detailed here for the benefit of any researchers who may be interested in pitfalls we encountered along the way. A rough scheme of the progression of the system is shown below.

## Supplementary Information

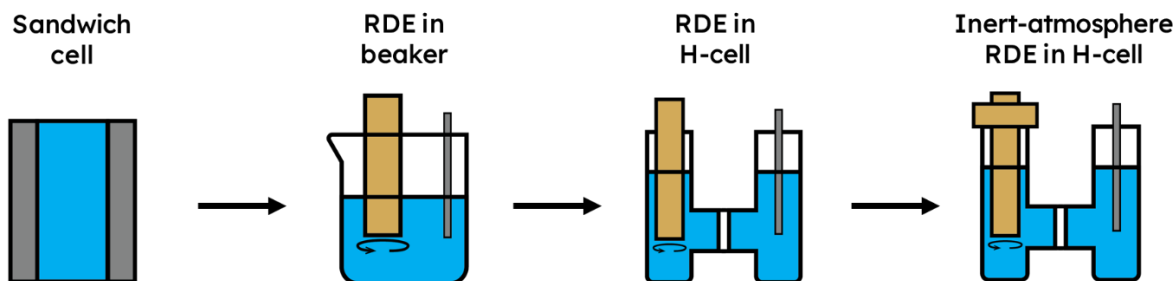


Figure S22. Experimental setup progression during troubleshooting phase.

At the outset, we started with a symmetric cell setup in sandwich configuration, with Pt foils as both anode and cathode. While this setup was conducive to online H<sub>2</sub> quantification, it also yielded high values of HER Tafel slopes (>300 mV/dec), even on Pt. We concluded that there were substantial transport limitations at play, and switched to an RDE configuration in a glass beaker cell.

While using the beaker cell, we were able to obtain higher current densities, as the rotation of the electrode allowed for more facile transport of reactants to the surface and products away from the surface. It was at this time that we noticed, however, that current would decrease substantially over time at a constant potential. Hypothesizing that this might be due to interference from the counter reaction, we returned to the sandwich cell and attempted to quantify gas-phase products from the oxidative reaction on the Pt wire counter-electrode. We found that at the various potentials tested, the counter electrode consistently produced a very small amount of carbon monoxide from the oxidative breakdown of acetonitrile in the presence of water. We hypothesize that this CO poisoned the surface of the Pt working electrode, leading to a decrease in HER current over time. This issue was solved by the separation of the working electrode and counter electrode by a glass frit in an H-cell configuration.

Once in the H-cell configuration, currents were steadier over time and Tafel slopes for HER were much lower. However, at this point it became apparent from LSV experiments that some amount of background current existed. The current was reductive, with current densities on the order of -1 mA/cm<sup>2</sup> when the electrode was spun at 1600 RPM with no gas purge through the working compartment. By experimenting with purging inert gas into the working electrolyte, we were able to observe substantial decreases in background current when O<sub>2</sub> was excluded from the electrolyte. As a result, a gas-purged bearing compatible with the RDE was purchased, and a custom H-cell was ordered to provide the proper seal. At this point we arrived at the final set of methods reported in this work. With this setup, a background of only ~0.05 mA/cm<sup>2</sup> ORR persisted. Decreasing the background current in this way was necessary in order to observe reasonable Tafel slopes for HER.

It should be noted that, in addition to purging N<sub>2</sub> and Ar, we also attempted to purge H<sub>2</sub> through the system. The reasoning for this is similar to the reasoning behind the purging H<sub>2</sub> during the OCV measurement experiments; having the product of the reaction present at a defined activity makes the reaction better thermodynamically defined. Because H<sub>2</sub> is such a light gas, however, the H<sub>2</sub> purge in general took longer to achieve the same effectiveness as Ar at excluding O<sub>2</sub>, especially

when H<sub>2</sub> was not introduced directly through the electrolyte but rather through the headspace. We were unable to remove O<sub>2</sub> to acceptably low levels using the H<sub>2</sub> purge alone. For this reason, the experiments reported in this work rely on Ar, a heavier gas, to remove the O<sub>2</sub> from solution and eliminate background ORR current.

### Discussion: Local Tafel slopes & sensitivity of Tafel slope to fit range

By taking a point-to-point instantaneous slope in the HER LSV data set and smoothing it using a 41-point moving average, we were able to plot the approximate local Tafel slope at each potential. (Figure S23) Note: there is no inherent significance to the 41-point average; this value was chosen for visual smoothness.

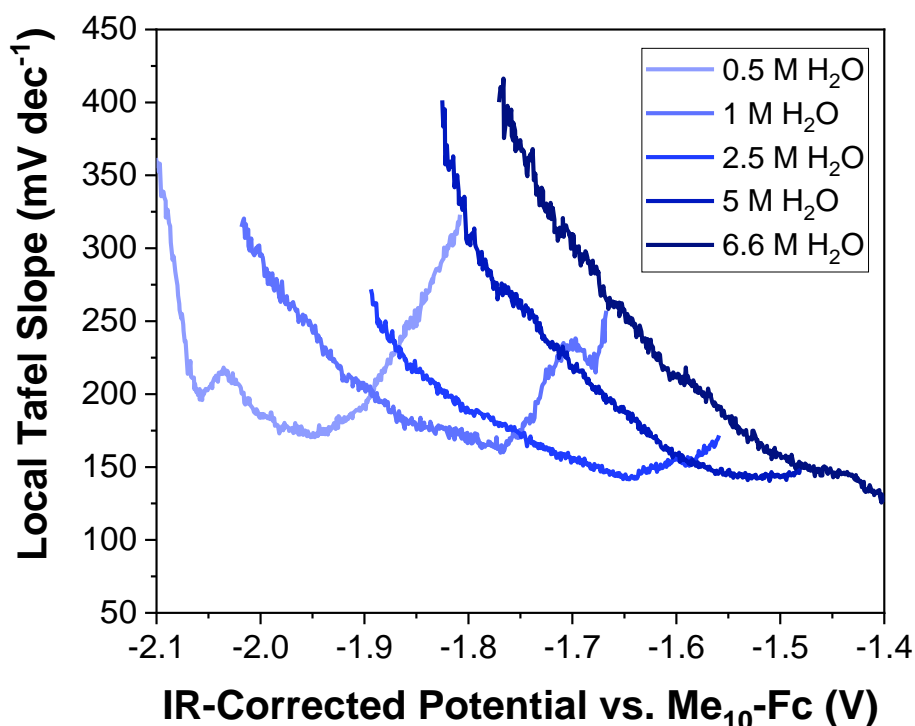


Figure S23. Local Tafel slope for HER on Au in the potential range studied. Note: Tafel data at higher currents were noisy; therefore, the local data reported here are cut off prior to the end of the data set, for clarity.

In each trace, as the Au electrode is negatively polarized, the measured current comes off of the small ORR plateau and potential has an increasing effect on rate (i.e. a lower Tafel slope). This is followed by a minimum in measured Tafel slope and an ensuing steady increase as a variety of factors (transport, Marcus-like kinetics, etc.) begin to play a larger role.

Because of the density of data points used in collecting the Tafel data, it was unreasonable to report errors in Tafel slope estimated from fitting that data, as they are artificially deflated by an abundance of data points. However, we were also unable to use the Bayesian data analysis approach developed previously<sup>17</sup> to fit the full data set, as this approach has difficulty dealing with

## Supplementary Information

phenomena such as background current. Instead, we have opted to tabulate here how the reported Tafel slope would change with slight changes in the fit region. Note that we have not altered the width of the fit region, which is 1 decade of current in all cases.

Table S4. Sensitivity of Tafel slope to fit range

Concentration H <sub>2</sub> O (M)	Reported TS fit start (log (i / mA cm <sup>-2</sup> ))	Reported TS fit end (log (i / mA cm <sup>-2</sup> ))	Reported TS (mV/dec)	TS 0.1 decade earlier	TS 0.1 decade later
0.5	-0.5	0.5	183.4	186.1	184
1	-0.6	0.4	172.1	176.4	172.4
2.5	-0.6	0.4	148	148.9	148.4
5	-0.6	0.4	144.5	145.1	144.8
6	-1	0	130.4	132.2	130.6

The Tafel slope is relatively insensitive to fit range within this window, changing by less than 5 mV/dec with a shift of 0.1 dec in either direction.

### **Discussion: Water dependences of HER in blended electrolyte at different potentials**

There was a small window in which we could make comparisons of HER rate across most water activities. The following plots represent constant-potential cuts (w.r.t. Me<sub>10</sub>-Fc) through the same data set, made at different potentials than the one reported in the main text. Data for which total current density was lower than ~0.75 mA/cm<sup>2</sup> was discarded as there was likely too much interference from the ORR background.

Supplementary Information

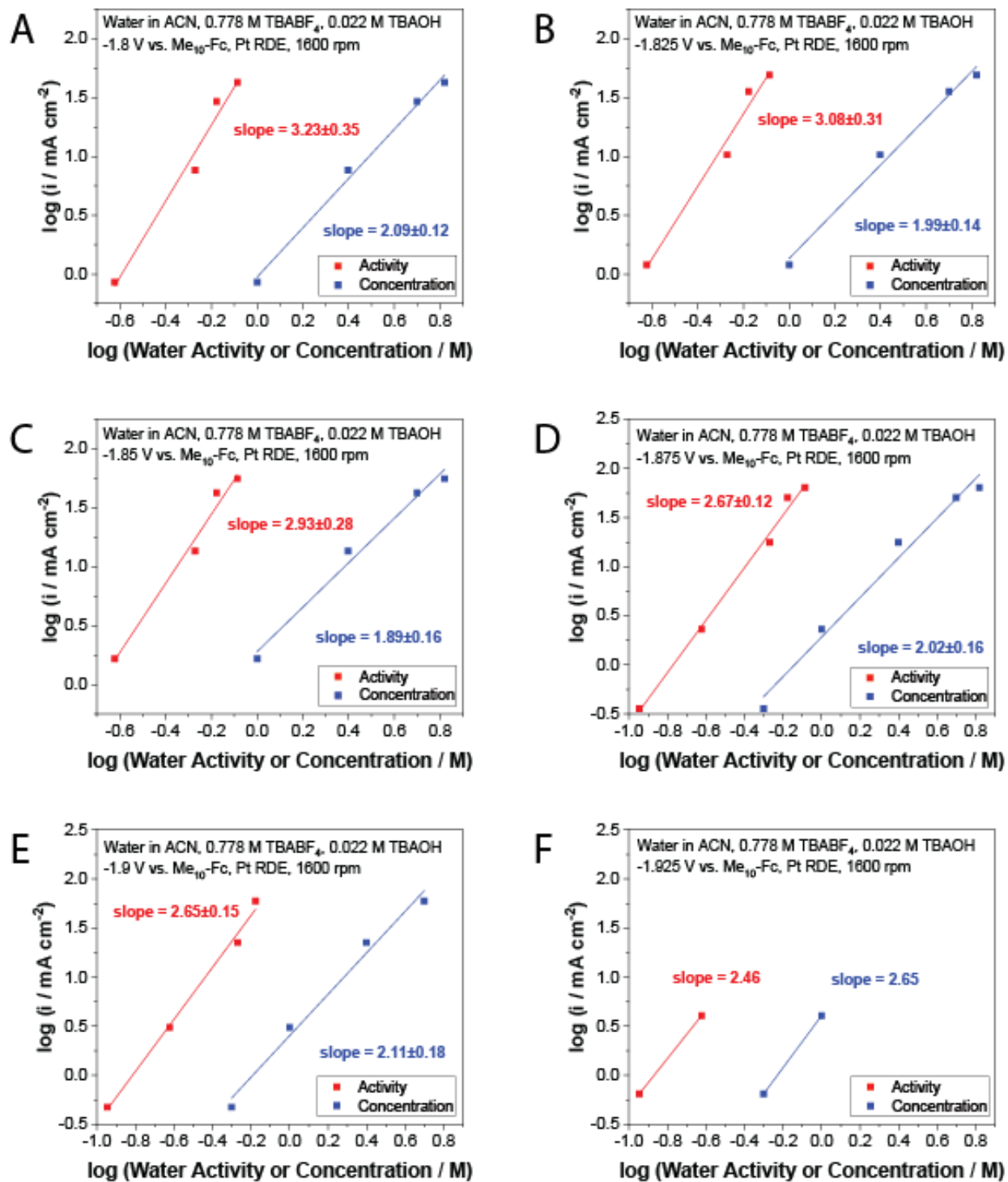


Figure S24. Water dependences of HER on Au at multiple potentials: A) -1.8 V vs. Me<sub>10</sub>-Fc, B) -1.825 V vs. Me<sub>10</sub>-Fc, C) -1.85 V vs. Me<sub>10</sub>-Fc, D) -1.875 V vs. Me<sub>10</sub>-Fc, E) -1.9 V vs. Me<sub>10</sub>-Fc, F) -1.925 V vs. Me<sub>10</sub>-Fc.

Data shown in the main text – the plot at -1.875, here also shown with an additional lower-concentration data point (Figure S24D) – was selected so that the broadest range of water concentrations could be compared at a single potential. Because the water dependence across this range of potentials is similar, we can say that the data selected for inclusion in the main text is fairly representative of the full data set, and that the analysis would not change drastically if we had selected a slightly different potential.

In all cases, the linear fits to the activity data are fairly strong. In addition, we can observe an interesting trend: there is an apparent decrease in water dependence with decreasing potential (increasing overpotential). At the same time, the discrepancy between measured water dependence with respect to concentration versus activity decreases as potential becomes more reductive – although this is at least partially due to the concentration range being compared.

### **Discussion: Sources of errors (accounted and unaccounted) in HER water dependence data**

The errors accounted for in main text Figure 2C, the water dependence of HER in the acetonitrile-water blended electrolyte, are the following:

- X-error: error from triplicate activity measurements (no x-error reported for concentration data)
  - This is the same as error shown in Figure 2A, shifted into the log space.
- Y-error: error estimated from the process of averaging the oxidative and reductive peaks during Me<sub>10</sub>-Fc calibration
  - This potential error from calibration was propagated through to the LSV data to yield errors in measured current. Note that it is relatively small compared to X-error on activity data set.

Known errors that are *not* accounted for, either because they are difficult to accurately quantify or because they likely contribute little to the results, include:

- Temporal changes in electrolyte composition throughout the HER run due to evaporation
  - Because the system was open, some amount of electrolyte was able to evaporate during the run. Since acetonitrile is the most volatile system component, followed by water, it stands to reason that the electrolyte left to evaporate would increase both in water concentration and in ionic strength over time. However, typical volume losses for recovered electrolyte over the course of a ~4-hour experiment were roughly 3 mL, about 10% of the total electrolyte volume and no more than 20% of the working electrolyte volume. Actual electrolyte losses at the time of the reported LSV were likely substantially less than this.
- Temporal changes in the reference throughout the HER run, and corresponding differences in potential
  - From the measured OCV data, we know that the junction behavior of the “leak-free” Ag/AgCl pseudoreference changes over time. Depending on the electrolyte

and the state of the reference, it appears that potential behavior can shift at different rates as well. (Figure S17) This is why, despite the LSV experiments being shorter than the reported OCV measurement experiments, and despite the LSVs for all compositions taking place at nearly identical time points after the start of the corresponding experiment (1.5 hours), there is still considerable uncertainty in how the behavior of the pseudoreference contributed to errors in water dependence measurements. However, looking at LSVs immediately following those reported in Figure 2B (see Figure S14, as the rotation rate dependence experiments were conducted in the following 2 hours, in the order 1600 RPM – 900 RPM – 2500 RPM), we can see that HER takeoff occurs around the same potential at each time point, suggesting that the reference is reasonably stable in the working electrolyte, and therefore this source of error is relatively small. Perhaps coincidentally, the largest change over time is observed in the 1 M water experiment, for both the sequential LSVs (Figure S14) as well as for the OCV measurements. (Figure S17)

- Any run-to-run differences for a given electrolyte composition
  - Because only one data set for each electrolyte is used to draw the conclusions here, we did not account for error between runs. However, replication experiments completed within the lab using different pseudoreference electrodes yielded similar Tafel slopes and water dependences as those reported here.
- Instrumental errors from electrolyte formulation
  - This can be calculated from reported errors for pipettes used in making electrolytes, but such errors tend to cancel and should be negligibly small.

### Discussion: On curvature in order-dependence data

We wish to stress once again that linearity should absolutely not be expected from order-dependence data *a priori*. It is interesting to note, however, that at essentially every ET-referenced potential shown here, the activity correction does serve to make water dependence data more linear. One way to show this mathematically is to look at the residuals of the linear fits for the concentration-based and activity-based data. If a data set is fairly linear, the residuals will scatter around the fit without a trend. On the other hand, if there is curvature in the data, the residuals will exhibit obvious curvature, with a parabolic shape. We show a representative visualization for the HER water dependence data here.

## Supplementary Information

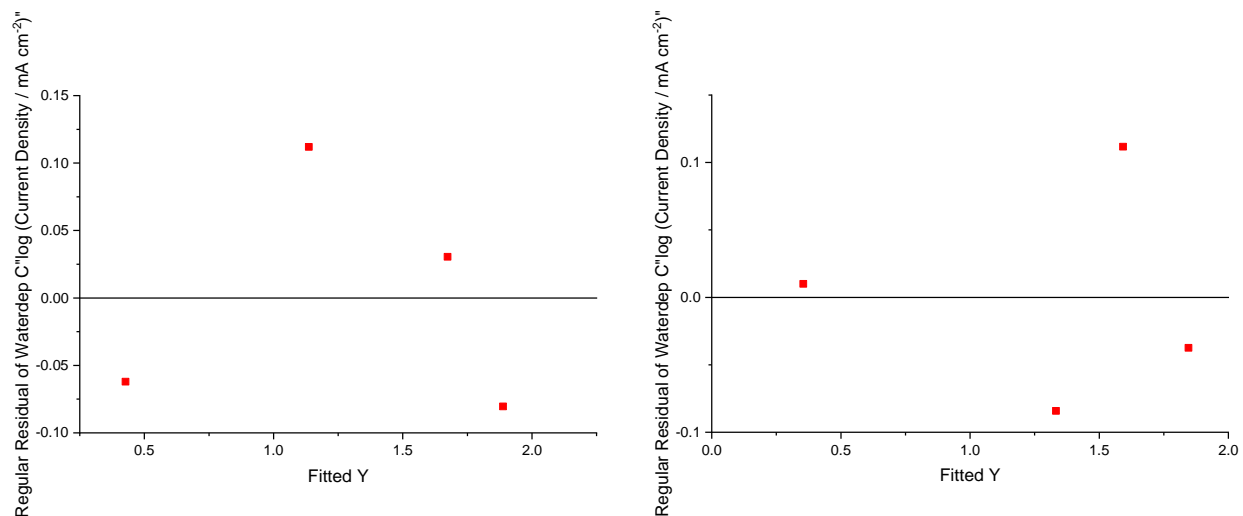


Figure S25. Residuals of fit for HER water dependence data in the case where the x-axis is  $\log(\text{concentration})$  (left) and  $\log(\text{activity})$  (right).

### Discussion: Water movement across the glass frit

It was noted that during hydrogen evolution experiments on the RDE with electrolytes containing a high activity of water – i.e. the 6.6 M condition – the counter-electrolyte would cloud up and phase-separate as the experiment progressed, indicating that water activity exceeded unity in this compartment. We hypothesize that because the cell was operated under basic conditions, the primary ionic charge carrier was  $\text{OH}^-$  – and as this  $\text{OH}^-$  diffused/migrated toward the anode during operation, it brought with it a solvation shell containing mostly water. For this reason, there is some transiency to the electrochemical measurements – water activity may be slightly decreasing in the working electrolyte over time. (This balances with electrolyte evaporation, however, which favors vaporization of acetonitrile – therefore, it is hard to predict the nature of the transient change in water activity. This could of course be directly measured through HS-GC-TCD.)



Figure S26. Phase separation observed in anolyte of H-cell during HER at high- $a_{\text{H}_2\text{O}}$  conditions.

**Discussion: Effect of water content on organic substrate activity for OAT reactions**

While quantifying water activity for the OAT electrolytes, we were also able to quantify activity for the OAT substrates (cyclooctene, cyclohexanone) with changing water content. A plot of cyclohexanone peak area vs. electrolyte water content is shown here.

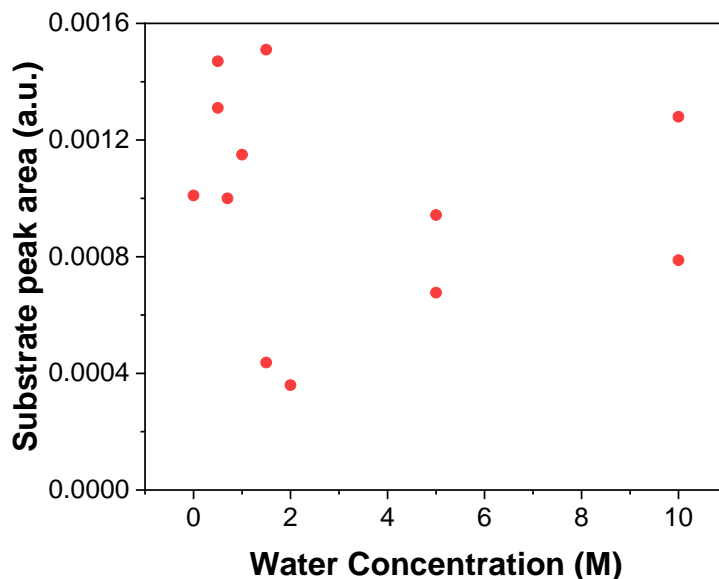


Figure S27. Cyclohexanone substrate HS-GC-TCD peak area versus lactonization electrolyte water content.

Unfortunately, likely due to the low volatility of the organic substrates, the spread on these measurements was fairly large. It was difficult to assess whether there was a trend in cyclohexanone activity with water content from this data set alone.

In the case of cyclooctene, only two data points were collected: one at low water content and one at 12.5 M water. In line with our intuition that increasing water content should increase the activity of hydrophobic cyclooctene, the peak area for the 12.5 M water case was 3.4 times larger than the substrate peak area in a 0 M water electrolyte. However, this difference is on the same order as the spread in the cyclohexanone data, so results here too are inconclusive.

**SI References**

- (1) Williams, K.; Corbin, N.; Zeng, J.; Lazouski, N.; Yang, D.-T.; Manthiram, K. Protecting Effect of Mass Transport during Electrochemical Reduction of Oxygenated Carbon Dioxide Feedstocks. *Sustain. Energy Fuels* **2019**, *3* (5), 1225–1232.
- (2) Li, Q.; Batchelor-McAuley, C.; Lawrence, N. S.; Hartshorne, R. S.; Compton, R. G. Anomalous Solubility of Oxygen in Acetonitrile/Water Mixture Containing Tetra-n-Butylammonium Perchlorate Supporting Electrolyte; the Solubility and Diffusion

## Supplementary Information

- Coefficient of Oxygen in Anhydrous Acetonitrile and Aqueous Mixtures. *J. Electroanal. Chem.* **2013**, 688, 328–335.
- (3) Goyal, A.; Marcandalli, G.; Mints, V. A.; Koper, M. T. M. Competition between CO<sub>2</sub> Reduction and Hydrogen Evolution on a Gold Electrode under Well-Defined Mass Transport Conditions. *J. Am. Chem. Soc.* **2020**, 142 (9), 4154–4161.
  - (4) Dubouis, N.; Serva, A.; Berthin, R.; Jeanmairret, G.; Porcheron, B.; Salager, E.; Salanne, M.; Grimaud, A. Tuning Water Reduction through Controlled Nanoconfinement within an Organic Liquid Matrix. *Nat. Catal.* **2020**, 3, 656–663.
  - (5) York, D.; Evensen, N. M.; Martínez, M. L.; De Basabe Delgado, J. Unified Equations for the Slope, Intercept, and Standard Errors of the Best Straight Line. *Am. J. Phys.* **2004**, 72 (3), 367–375.
  - (6) Wiens, T. Linear Regression with Errors in X and Y <https://www.mathworks.com/matlabcentral/fileexchange/26586-linear-regression-with-errors-in-x-and-y> (accessed Jan 12, 2022).
  - (7) Treiner, C.; Tzias, P.; Chemla, M. Solvation of Tetrabutylammonium Bromide in Water Acetonitrile Mixtures at 298.15 K from Vapour Pressure Measurements of Dilute Solutions. *J. Chem. Soc. Faraday Trans. 1* **1976**, 72, 2007–2015.
  - (8) Sirotkin, V. A.; Solomonov, B. N.; Faizullin, D. A.; Fedotov, V. D. IR Spectroscopic Study of the State of Water in Dioxane and Acetonitrile: Relationship with the Thermodynamic Activity of Water at 278–318 K. *J. Struct. Chem.* **2000**, 41 (6), 997–1003.
  - (9) Jin, K.; Maalouf, J.; Lazouski, N.; Corbin, N.; Yang, D.; Manthiram, K. Epoxidation of Cyclooctene Using Water as Oxygen-Atom Source at Manganese Oxide Electrocatalysts. *J. Am. Chem. Soc.* **2019**, 141 (15), 6413–6418.
  - (10) Maalouf, J.; Jin, K.; Yang, D.; Limaye, A.; Manthiram, K. Kinetic Analysis of Electrochemical Lactonization of Ketones Using Water as the Oxygen Atom Source. *ACS Catal.*
  - (11) Madon, R. J.; Iglesia, E. Catalytic Reaction Rates in Thermodynamically Non-Ideal Systems. *J. Mol. Catal. A Chem.* **2000**, 163 (1–2), 189–204.
  - (12) Lowe, B. M.; Skylaris, C. K.; Green, N. G. Acid-Base Dissociation Mechanisms and Energetics at the Silica-Water Interface: An Activationless Process. *J. Colloid Interface Sci.* **2015**, 451, 231–244.
  - (13) Harris, J.; Kasemo, B. On Precursor Mechanisms for Surface Reactions. *Surf. Sci.* **1981**, 105, L281–L287.
  - (14) Durst, J.; Simon, C.; Hasché, F.; Gasteiger, H. A. Hydrogen Oxidation and Evolution Reaction Kinetics on Carbon Supported Pt, Ir, Rh, and Pd Electrocatalysts in Acidic Media. *J. Electrochem. Soc.* **2015**, 162 (1), F190–F203.
  - (15) Haghghat, S.; Dawlaty, J. M. PH Dependence of the Electron-Transfer Coefficient: Comparing a Model to Experiment for Hydrogen Evolution Reaction. *J. Phys. Chem. C* **2016**, 120 (50), 28489–28496.

## Supplementary Information

- (16) Goyal, A.; Koper, M. T. M. Understanding the Role of Mass Transport in Tuning the Hydrogen Evolution Kinetics on Gold in Alkaline Media. *J. Chem. Phys.* **2021**, *155* (13).
- (17) Limaye, A. M.; Zeng, J. S.; Willard, A. P.; Manthiram, K. Bayesian Data Analysis Reveals No Preference for Cardinal Tafel Slopes in CO<sub>2</sub> Reduction Electrocatalysis. *Nat. Commun.* **2021**, *12* (1), 1–10.
- (18) Zheng, J.; Yan, Y.; Xu, B. Correcting the Hydrogen Diffusion Limitation in Rotating Disk Electrode Measurements of Hydrogen Evolution Reaction Kinetics. *J. Electrochem. Soc.* **2015**, *162* (14), F1470–F1481.
- (19) Roberts, J. A. S. S.; Bullock, R. M. Direct Determination of Equilibrium Potentials for Hydrogen Oxidation/Production by Open Circuit Potential Measurements in Acetonitrile. *Inorg. Chem.* **2013**, *52* (7), 3823–3835.
- (20) Wise, C. F.; Agarwal, R. G.; Mayer, J. M. Determining Proton-Coupled Standard Potentials and X-H Bond Dissociation Free Energies in Nonaqueous Solvents Using Open-Circuit Potential Measurements. *J. Am. Chem. Soc.* **2020**, *142* (24), 10681–10691.
- (21) Agarwal, R. G.; Coste, S. C.; Groff, B. D.; Heuer, A. M.; Noh, H.; Parada, G. A.; Wise, C. F.; Nichols, E. M.; Warren, J. J.; Mayer, J. M. Free Energies of Proton-Coupled Electron Transfer Reagents and Their Applications. *Chem. Rev.* **2021**.